ATL-MUON-PUB-2007-003
17 April 2007

ATLAS 2004 Combined Test Beam results: Muon Chamber Alignment and Muon Reconstruction

F. Bauer, L. Chevalier, J. Ernwein, A. Formica, P.-F. Giraud, C. Guyot, S. Hassani, A. Krepouri*, E. Lançon, J.-F. Laporte, R. Nicolaidou, A. Ouraou, P. Ponsot, P. Schune

CEA-Saclay, DAPNIA, F-91191 Gif-sur-Yvette, France

Abstract

In 2004, a combined systems test was performed in the H8 beam line at the CERN SPS with the following ATLAS detectors: the Inner Detector, the Liquid Argon Calorimeter, the Tile Hadronic Calorimeter and the Muon Detectors. This note describes results obtained for the alignment of the Monitored Drift Tube (MDT) chambers in the Muon Detectors setup, the performance of the MDT chambers and the reconstruction of muon tracks using the combined information from both the Inner Detector and the Muon Spectrometer.

---

* *On leave of absence from the University of Thessaloniki*

1. Introduction

The muon spectrometer **[1]** of the ATLAS detector was designed to provide a stand-alone trigger for muons with transverse momentum of several GeV as well as a measurement of final state muons with a momentum resolution of about 3% over most of the momentum range. A resolution of 10% is expected for a transverse momentum p_T of 1 TeV. The muon spectrometer is a 4π detector, which consists of four types of detector technologies. Over most of the spectrometer acceptance, Monitored Drift Tube (MDT) chambers are used for the precision measurement of muon tracks. The MDTs are made of gas filled aluminum tubes with a central wire and measure charged particle tracks with an average spatial resolution better than 80μm. Cathode Strip Chambers (CSC) are used instead in the inner part of the end-cap regions where the background rate is very high.

Three stations of Resistive Plate Chambers (RPC) provide the trigger for muons in the barrel region whereas three Thin Gap Chamber (TGC) stations serve the same purpose in the higher background region of the end-cap. The signals from the trigger chambers are amplified, discriminated and digitized on the detector and sent to ASIC-based coincidence matrix boards. These boards perform the functions needed for the trigger algorithms and apply the p_T cuts according to preset thresholds. The trigger chambers are also used to provide the coordinate along the drift tubes (the "second coordinate"), which is not measured by the MDT chambers. Several additional TGC chambers are installed close to the end-cap inner MDTs and serve the same purpose of improving the measurement of this coordinate.

The muon momentum measurement is based on the measurement of three points along the track of the particle that is deflected in the magnetic field. The curvature is a measure of the particle momentum. Each of the three *stations* in the muon barrel system provides one measurement point along the track. It is convenient to express the curvature in terms of the *sagitta*, which is the distance from the point measured in the middle station to the straight line connecting the points in the inner and outer stations. The precision of the sagitta measurement is a direct measure of the precision of the muon momentum. A muon of momentum 1TeV/c has a sagitta of about 500 μm, and the target momentum measurement precision of 10% requires a sagitta precision of 50 μm. The actual precision depends not only on the local precision of the points measured in the muon chambers, but also on the relative positions of the three stations. These positions need therefore to be known with an accuracy that is comparable to the individual chamber point measurement precision. The total contribution of the chamber point measurements to the sagitta precision should be less than 40 μm. It is impossible to keep the geometry of the chambers stable within that precision; alignment systems are therefore needed to continuously monitor the relative chamber positions with high accuracy, especially for the displacements in the sagitta direction which are of prime importance. These requirements lead to the alignment scheme outlined in section 3, which aims at a 20 μm total contribution of the alignment to the uncertainty of the sagitta measurement.

A large-scale test stand of ATLAS detectors, including all the muon spectrometer components was operating at CERN in the H8 beam line from 2000 to 2004. A particle beam of momentum up to 350 GeV from the SPS accelerator was used to study various aspects of the spectrometer. In this note we summarize the performance of the muon system and its components during the 2004 H8 test period.

The note is organized as follows: the experimental set-up of the 2004 ATLAS combined test beam is described in section 2. In section 3 the alignment concept of the MDT chambers, the specific installation of the H8 alignment components and the method used for analysing the measurements from the optical sensors are described. Section 4 reports on the analysis framework and the data samples analysed for our studies; a short description of the muon reconstruction software as well as the method which was developed for the sagitta computation is also presented in this section. In section 5 the alignment results are reported; results related to the monitoring of the optical sensors can be found in section 5.1 and the results related to the controlled chamber movements in section 5.2. Section 6 deals with the chamber alignment using straight tracks. Finally, section 7 describes the results obtained for segment and track reconstruction in the test beam environment: results for track segment and single hit efficiencies of MDT chambers are presented in section 7.1, followed by results on combined tracking with the inner detector and the muon spectrometer information in section 7.2.

2. Experimental setup

The setup of the 2004 ATLAS Combined Test Beam (CTB), as shown in Figure 1, consists of four parts: the inner detector, the calorimeters, the muon detectors and the beam line elements. In this combined test-beam, a full slice of all barrel ATLAS detectors was tested for the first time and many systems were already in their final production version.

In the combined test beam, the inner detector consisted of three layers of silicon pixel modules, four layers of two silicon strip detectors (SCT) and two wedges of the straw drift tube detector (TRT). The Liquid Argon (LAr) electromagnetic calorimeter module and the hadronic calorimeter (TileCal) modules were both placed on a table which could be rotated and translated to expose specific cells to the beam**.**

The dump between H8A and H8B was a block of iron of 3200 mm along the beam direction and with a transverse area of 800 mm^2. It was kept in place for most of the data taking. A detailed description of the CTB setup can be found in **[2].**

The H8 muon stand shown in Figure 2, had two parts, a barrel stand and an end-cap stand. The barrel setup reproduced one ATLAS barrel sector with its MDT and RPC stations. It consisted of six MDT chambers, two of each type: inner (BIL), middle (BML) and outer (BOL) chambers, fully instrumented with Front End electronics (FE) read out with a Muon Readout Driver (MROD) and fully equipped with an optical alignment system. Each MDT triplet (BIL, BML, BOL) formed an ATLAS-like tower. In the barrel setup there were six RPC doublets: four middle chambers (BML) and two outer chambers (BOL). Three additional stations were installed in the test stand: one inner station (BIL) placed on a rotating support for calibration studies, one outer (BOS) station (MDT+RPC) upstream of the muon wall for noise and Combined Test Beam (CTB) studies and one inner station (BIS) placed in front of the Liquid Argon Calorimeter for electrode positioning studies.

In the end-cap stand, which reproduced a muon spectrometer end-cap sector, there were 6 MDT chambers (Small and Large): two inner (EI), two middle (EM) and two outer (EO). As in the barrel they were fully instrumented with FE and read out through one MROD.

The chambers were equipped with the complete alignment system and calibrated sensors for absolute alignment. For triggering in the end-cap, there were three TGC units: one triplet and two doublets fully instrumented with on-chamber electronics.
Three bending magnets namely MBPSID, MBPL, and MBPS2 were used during different periods. Both the pixel and the SCT were located inside the magnetic field of the MBPSID magnet, whereas the TRT was installed outside the magnet. The orientation of the field was horizontal in order to deflect particles vertically. The MBPL magnet was installed in front of the muon barrel stand and was used to bend tracks horizontally. This magnet was operated with various currents and both polarities. The MBPS2 magnet was installed between the EI and the EM of the end-cap muon setup to measure the muon momentum.
The CTB reference system is chosen as similar as possible to the ATLAS reference system. The x-axis is along the H8-beam, the z-axis is horizontal and the y-axis is vertical to form a direct orthogonal reference frame. The point x=y=z=0 is on the axis of the H8 beam, at the entrance surface of the inner detector magnet (MBPSID). This system, (shown in Figure 36), will be used throughout this note.
Two external trigger systems were available; a small area trigger system given by the coinsidence of two scintillators of 10 x 10 cm^2 centered on the beam line and a large area system trigger of 60 x 100 cm^2, (called hodoscope trigger), given by the coinsidence of the signals of two planes of six scintillating slabs of 10 x 100 cm^2 each.

3. Alignment of MDT chambers

3.1. The alignment devices

The ATLAS muon alignment system is based on optoelectronic sensors that measure the relative positions and the deformations of the MDT chambers. In addition, temperature sensors monitor their global thermal expansions.
In the barrel part, the optical sensors are placed directly on the chambers, whereas the alignment of the end-cap part makes use of a set of intermediate optically and temperature controlled aluminium bars carrying optical sensors to measure their relative positions and to relate them to neighbouring chambers.
Two types of sensors are used: a 3-point alignment device, the RASNIK **[3]** (Read Alignment System of NIKhef) and a camera system (SAclay CAMera (SACAM) in the barrel and a Boston Ccd Angle Monitor (BCAM) **[4]** in the end-cap). In the RASNIK system, the image of a back lighted chessboard mask, precisely located on a first element to be aligned, is projected on a CMOS (barrel) or CCD (end-cap) image sensor located on the third element to be aligned through a lens located on the second element to be aligned. It measures precisely (to a few microns) the departure from a straight line of the transverse position of the 3 optical elements, and less precisely (to a few hundred microns) their relative position along the optical axis by using the magnification. In the 2-point camera system, the CMOS or CCD camera located on a first element captures the image of a set of LEDS precisely placed on a second element. It measures precisely (to a few micro radians) the bearing angle of the second element viewed from the first one.

3.2. The barrel alignment setup of H8

The MDT chamber deformations are monitored by a set of 4 *inplane* RASNIK systems connecting the 3 cross plates which are the structural elements holding the multilayers of tubes.
The relative positions of two adjacent chambers are measured by two *praxial* systems, each one made of two short RASNIK sensors at the edges of the tube multilayers, and one *axial* RASNIK system spanning the full width of the two chambers.
The relative position of the 3 layers of BIL, BML and BOL chambers is controlled by 8 *projective* RASNIK systems, which mimic the behaviour of straight particles crossing the chambers close to their corners. The mask is placed on BIL, the lens on BML and the image sensor on BOL chambers.
In addition to the *projective* system, the 3D chamber position measurement is improved for some of its parameters (mainly for angular relative orientation and for position along the beam direction) by a so-called *reference* system which consist of a set of 4 stiff aluminum plates, each carrying 4 SACAM camera systems which optically interconnect the plates and connect the plates to neighbouring chambers.
A CAD visualization of the setup is shown in Figure 3. Table 1 provides the list of optical lines (RASNIK and SACAM) in the H8 setup. This setup corresponds to about 1% of ATLAS. Compared to a double tower in ATLAS which contains only 4 projective lines, 4 additional projective lines have been added in H8 at intermediate polar angles in order to better control the systematic effects induced by a reduced number of lines.

Name	Sensor type	Number of sensors	Alignment type
In-plane	RASNIK	24	MDT deformations
Praxial	RASNIK	12	Plane alignment
Axial	RASNIK	6	Plane alignment
Projective	RASNIK	8	Tower alignment
Reference	SACAM	16	Alignment wrt. the toroid

Table 1: The optical systems used in the H8 barrel alignment setup.

3.3. The end-cap alignment setup of H8

The alignment setup **[5]** corresponds to one octant of an end-cap side of the ATLAS muon spectrometer (about 2% of the ATLAS system). It consists of a set of 6 optically controlled aluminium bars, 2 per chamber layer (EI, EM and EO). Each bar shape is controlled by 3 interspersed RASNIKs systems. In addition, the bar sagitta is measured by 2 BCAM cameras located at both ends of the bar and looking at each other. The relative position of the bars is measured by BCAMs: *polar* BCAMs connect bars of different layers; *azimuthal* BCAMs connect bars of the same layer. The MDT chambers are linked to the neighbouring bars through RASNIK systems (CCD/lens on the chamber, mask on the bar). As there are only 2 bars to control the position of small and large chambers (e.g. EMS and EML), additional BCAM monitors have been added on a chamber, at roughly mid distance between the 2 bars in order to control the relative angle of the 2 chambers (the so-called saloon door effect). The total number of systems of each type in the H8 setup is given in Table 2 and a schematic view of the setup is shown in Figure 4.

Name	Sensor type	Number of optical lines	Alignment type
In plane	RASNIK	24	MDT deformations
Bar Monitor	RASNIK	20	Bar deformations
Radial	BCAM	12	Bar deformations
Polar	BCAM	24	Bar to bar connections
Azimuthal	BCAM	12	Bar to bar connections
Proximity	RASNIK	15	Chamber to bar connections
Saloon Door	BCAM	12	Chamber to bar connections

Table 2: The optical systems used in the end-cap alignment setup

3.4. Alignment reconstruction

3.4.1. ASAP reconstruction program

The geometry reconstruction software ASAP **[6]** (**A**tlas **S**pectrometer **A**lignment **P**rogram) has been developed in order to translate the optical sensor measurements into MDT positions and deformations in the barrel area. It is written in C++ using ROOT libraries, visualisation tools and XML interfaces. It uses the description of the geometry, the positions of the optical sensors and their calibration constants and provides the positions and distortions of the MDT chambers using standard fitting methods.

3.4.2. ARAMYS reconstruction program

For the alignment of the end-cap chambers the corresponding program is ARAMYS ('**A**lignment **R**econstruction and Simulation for the **A**tlas **Mu**on **S**pectrometer') [**7**]. The program implements the description of alignment bar deformations based on forces as well as MDT chamber deformations. It uses a description of the geometry of the setup and a sensor database generated from various calibration sources. It is written in C and relies on the CERN minimization software MINUIT to find the set of positions and deformations of the objects that is in best agreement with a given set of sensor measurements.

3.4.3. Alignment modes

Two alignment modes (relative and absolute) are possible and were tested in the muon H8 setup.
In the *relative mode* it is assumed that the MDT chamber positions are known at a given time (these positions are input to the so-called *reference geometry*); the optical sensor responses are used to infer the subsequent chamber movements with a precision better than 20 μm.
In the *absolute mode* the position of the chambers is calculated using only the current measurements of the optical sensors; this mode requires an accurate calibration of all the alignment parts.

Both alignment modes are internal to either the barrel or the end-cap part of the muon spectrometer; in both the H8 setup and in ATLAS there is no information linking the aligned muon spectrometer to the other detectors. Particle tracks will have to be used for aligning, e.g., the inner detector and the muon spectrometer in ATLAS.

4. Data samples and analysis framework

4.1. Data samples

The analyses described in this note have been performed on a set of data collected during July and November 2004.
The characteristics of most of the analyzed runs are listed in Table 3.

July Period						
Run number	**Trigger**	**Beam Energy (GeV)**	**MDT threshold (mV)**	**MBPS current (A)**	**MBPL current (A)**	**Movements**
Alignment studies related to controlled movements of MDT chambers + alignment with tracks studies						
600520	Hodoscope		-40	0	0	BIL –8mrad in x
600522	Hodoscope		-40	0	0	BIL –6mrad in x
600523	Hodoscope		-40	0	0	Nominal
Track segment efficiency studies + alignment studies related to optical sensor monitoring						
600759	10x10	250	-40	0	600	Nominal
600760	10x10	250	-40	0	0	Nominal
600846	10x10	220	-40	0	0	Nominal
600860	10x10	220	-40	0	600	Nominal
600964	10x10	180	-40	0	600	Nominal
600967	10x10	180	-40	0	0	Nominal
600970	10x10	180	-44	0	0	Nominal
600978	10x10	180	-44	0	600	Nominal
600985	10x10	180	-52	0	600	Nominal
600985	10x10	180	-52	0	0	Nominal
600990	10x10	180	-36	0	0	Nominal
600993	10x10	180	-36	0	600	Nominal
November Period						
Run number	**Trigger**	**Beam Energy (GeV)**	**MDT threshold (mV)**	**MBPS current (A)**	**MBPL current (A)**	**Movements**
Track segment efficiency studies in presence of material						
2102574	10x10	180	-40	850	0	BOL2: 1mm in z
2102595	10x10	180	-40	850	0	BOL2: 1mm in z Stainless steel in front of BIL BML BOL

November Period						
Run number	**Trigger**	**Beam Energy (GeV)**	**MDT threshold (mV)**	**MBPS current (A)**	**MBPL current (A)**	**Movements**
Alignment studies related to controlled movements of MDT chambers						
2102562	10x10	180	-40	0	0	Nominal
2102568	10x10	180	-40	0	0	BOL2: 6mm in z
2102569	10x10	180	-40	0	0	BOL2: 4mm in z
2102617	10x10	180	-40	850	0	BOL2: 1mm in z BML2: 1mm in z, -1mrad in y BIL2: -2mrad in y
2102622	10x10	180	-40	850	0	BOL2: 1mm in z BML2: 1mm in z, -1mrad in y BIL2: 1.5 mm in z, -1mrad in y
2102628	10x10	180	-40	0	0	BOL2: 1mm in z BML2: 1mm in z, -1mrad in y BIL2: 3 mm in z, -1mrad in y
2102660	10x10	350	-40	0	0	BOL2: 2mm in z, -1mrad in y BML2: 5mm in z, 1mrad in y BIL2: -3mrad in y
2102667	10x10	350	-40	850	0	BOL2: 2mm in z, -1.8mrad in y BML2: 5mm in z, BIL2: 4 mm in z, 1mrad in y
2102671	10x10	350	-40	850	0	BOL2: 2mm in z, BML2: -1mm in z, -1mrad in y
Tracking and backtracking studies						
2102549	10x10		-40	0	0	Nominal
2102730	10x10 & 3x3	350	-40	850	200	BOL2: 2mm in z, BML2: -1mm in z,

Table 3: Characteristics of most of the analysed runs. Alignment studies related to the monitoring of optical sensors and to the controlled movements of MDT chambers were performed with additional runs not listed in this table.

4.2. Framework of analysis and muon reconstruction

In the H8 test-beam, a prototype of the full ATLAS software chain was tested to analyze the muon data. The reconstruction of the events was performed in the ATLAS offline framework ATHENA

In this framework, the various inputs (e.g response of optical alignment sensors) needed to run the reconstruction packages, are stored in a *Conditions Database* and are fed to the packages through dedicated services. A schematic view of the offline ATLAS muon reconstruction framework is shown in Figure 5, in which the full (dotted) lines indicate parts of the services that were (were not) implemented in the H8 offline setup respectively.

The necessary inputs of any muon reconstruction package are the calibration constants, the alignment corrections and the magnetic field map. The calibration constants (T0 and RT relation needed to make the transformation from time to radius of each reconstructed hit) [8] were produced for different configurations of H8 test-beam data, were written to ASCII files and fed to the reconstruction packages through

a dedicated "ATHENA service "; no link with the *Conditions Database* was established for H8 test-beam data. The alignment data, taken asynchronous to the test-beam data every 15 minutes, are written in the *Conditions Database* and provided the inputs to the alignment reconstruction packages (ASAP and ARAMYS) which operated outside ATHENA. After reading this information, these packages calculate the difference between the nominal detector geometry (provided by the Atlas Muon system DataBase AMDB **[9]**) and the actual geometry and write the result in the *Conditions Database*. A dedicated alignment service in ATHENA retrieves the result of the alignment from the condition database and feeds it to the reconstruction packages. Finally for the magnetic field, a dedicated service in ATHENA provides the map of the magnetic field at every point in space; no link with the *Conditions Database* existed at the time for the H8 reconstruction scheme.
The track pattern recognition program in this analysis is "*Muonboy*" using all muon chambers in the barrel and end-cap. In the test-beam, precision chambers (MDT) have their tubes in the vertical y-direction and measure only one coordinate with an accuracy of ~80 μm along the horizontal z-direction. Trigger Chambers (RPC, TGC) give the second coordinate (y-direction) with an accuracy of ~1cm. Tracking in the test-beam starts at 3100cm and ends at 5600 cm in the x-coordinate along the beam direction (Figure 6).
The pattern recognition in *Muonboy* proceeds sequentially according to the following scheme:

- Identification of 'regions of activity' (ROAs), guided by trigger chamber information
- Reconstruction of local straight track segments in each muon station belonging to a ROA
- Combination of track segments in different muon stations, to form muon candidate tracks
- Global re-fit of muon track candidates using individual hits.

Details concerning the algorithm can be found in **[1]**. Figure 6 shows the three locations (A, B, C) where the reconstructed track parameters and their full covariance matrices are provided.
The command parameters of *Muonboy* can be set to produce either straight track segments only, or they can be set to perform a full fit, which includes the effects of matter traversed and therefore provides fully reconstructed tracks.
Straight track segments were used in this note for the alignment studies and for the MDT efficiency analysis, whereas fully reconstructed tracks were used to perform the tracking and backtracking analyses. The computation of the sagitta in the H8 muon setup was the basic element of all the analyses performed with the straight track segments; details of this computation are given in the section below.

4.3. Sagitta computation

Throughout this section, a straight track segment produced by the *Muonboy* reconstruction package will be called "segment" for simplicity. A segment consists of two quantities: a 3D point located in the middle plane of the station and a 3D vector. The 3D point will be called *segment point* and noted *I*, *M* or *O* if it belongs to the Inner, Medium, or the Outer station, respectively. The 3D vector will be called *segment vector*.

In the middle plane of the station (parallel to the chamber wire plane) in which the segment point lies, it is convenient to define the second coordinate of the segment point along the ***t*** vector (the tube direction), and the first coordinate along the ***r*** vector, perpendicular to ***t*** (Figure 7).
We aim at a definition of the sagitta which does not depend on the second coordinate measurements. Thus, the distance of the segment point *M* to the straight line joining the segment points *O and I* is not convenient. Instead, the sagitta should be defined in a way that cancels the effect of displacements of segment points along the tube direction.
Assuming that the tube directions are parallel in the three stations, one finds that the only convenient sagitta definition is the one illustrated in Figure 8: the sagitta is the distance of point *M* to the plane defined by vectors *IO and t*, and containing *I*. The sagitta, which is then insensitive to displacements along the tube direction can be computed as:

$$s = \overrightarrow{IM} \bullet \frac{\vec{t} \wedge \overrightarrow{IO}}{\| \vec{t} \wedge \overrightarrow{IO} \|} \qquad (1)$$

In fact, tubes from different stations are not parallel and a sagitta for which the second coordinate measurements completely cancel out cannot be defined. However, even in this case, formula (1) indicates how the impact of these measurements can be minimized, provided that vector ***t*** is specified in connection with the three tube directions available.
If for example the tube direction is taken from the inner station, then the effect of the second coordinate measurement in this station will be canceled. If an average of the tube directions of the three stations is taken instead, then the effects of the second coordinate measurement in each station will be equally diminished, although none of the cancellations will be complete. In practice, it turned out that any particular choice among these options does not significantly affect the width of the sagitta distribution. We thus took the tube direction in the inner station while using formula (1)

4.4. Measurement of the second coordinate with MDT chambers

It is worth noting that if tubes from different stations are not parallel, the resolution of the second coordinate measurement contributes to the resolution of the sagitta. As an alternative to using RPCs for measuring the second coordinate, we developed a method, which uses MDT measurements only: we used segments measured in the end-cap stations to determine the second coordinates of segments in the barrel stations, and vice versa.
By definition, a segment measured in a station represents a track passing through the *segment point* along the direction of the *segment vector*. If we give up the second coordinate measurements for this segment, we can define a plane (the *segment plane)* containing the *segment point* and defined by the tube direction and the *segment vector*. This plane is shown in Figure 9.
By construction, the *segment plane* definition is neither sensitive to displacements of the *segment point* along the tube direction, nor to a component of the *segment vector* along this direction. With these two features, the *segment plane* does not depend on second coordinate measurements. A segment is therefore defined as a track lying in the *segment plane*, a constraint which is now independent of the second coordinate measurements used to build the segment.

The interest of using the *segment plane* appears clearly when combined with a second segment reconstructed in another station where the tube direction is different. Indeed it is then possible to correct the position of the point of this second segment by sliding it along this tube direction until it lies in the first segment plane, as illustrated in Figure 10.
This procedure can be seen from a more general point of view considering a pair of segments in a pair of stations. The intersection of the two *segment planes* forms a straight line, which is a direct prediction of the location of the track. Positions of both *segment points* can be corrected by translating the two original *segment points* until they reach this intersection. The *segment point* in the second station after correction shown in Figure 10 is one of these translated points.
It is worth commenting on the use of *segment vectors* in the above computations. As can be understood from Figure 10, the correction applied on a segment does not depend on its *segment vector*. On the other hand, as suggested by formula (1), the sagitta does depend only on positions, be they corrected or not. Thus, it follows that none of the *segment vectors* belonging to the segments are being used to compute the sagitta. The only *segment vector*, which enters the computations, is the vector of the segment used to determine the second coordinate of the others segments, e.g. the vector of the end-cap segment used to constrain the segments in the barrel.
The above manipulations makes sense only if one uses a geometry, which takes into account the alignment corrections. It is thus vital that a tool be available which provides alignment corrections. For the analyses presented here, we used the *AmdcRoot* application, which, in the framework of Root, provides the *Amdcsimrec* functionalities available in ATHENA.

5. Results on alignment with optical sensors

5.1. Optical sensor monitoring

During the 2004 test-beam period, a large amount of data provided by the alignment system of both the barrel and the end-cap muon stand were recorded. The continuous monitoring of a) chamber distortions and b) shifts of chamber positions relative to the global coordinates was made possible by the continuous data taking with the alignment system. In this section we present the variations of the relative positions of the chambers; they are due mostly to daily temperature variations and are reflected in the change of the mean value of the sagitta distribution. The sagitta was calculated separately in the barrel and the end-cap stand by considering straight track segments, as explained in section 4.3. The following quality criteria were applied in the reconstructed events: one segment per chamber was accepted with at least 7 (5) reconstructed hits for BIL/ EIL (BML, BOL/EML, EOL) respectively.
In Figure 11, the variation of the sagitta of reconstructed muon tracks in the end-cap stand for a period of one week is shown. Large variations, of the order of 500 μm, due to temperature variations (day/night effect), are visible on the left plot of Figure 11 which shows the sagitta distribution before applying the alignment corrections. These variations are reduced to around 80 μm when alignment corrections are made (right hand side plot of Figure 11). It is worth noticing here, that in the H8 setup the end-cap stand was closer to the door of the H8 hall and therefore subject to larger temperature variations than the barrel muon stand. For this reason the alignment corrections cannot account for all the temperature effects.

The mean values of the sagitta distribution in the end-cap calculated after applying the alignment corrections for the same one week period (i.e the mean values of the distribution shown in the right plot of Figure 11), is shown in Figure 12. The stability of the results is reflected in the RMS dispersion of this distribution which is of the order of 19 μm, well within specifications.
For the barrel stand the corresponding sagitta variations as a function of time are shown in Figure 13. In Figure 14 the sagitta distribution in the barrel muon stand is shown as a function of the temperature, before (left plot) and after (right plot) applying the alignment corrections. One can observe that for the barrel stand the temperature variations explain most of the sagitta variations.
A check of the stability and reproducibility of the results is shown in Figure 15. On the left plot the mean values of the sagitta distribution in the barrel muon stand are shown for a period of one week whereas on the right plot, the mean values are plotted for runs taken in a one month interval. One observes that the mean value of the sagitta in both plots is stable at the μm level.

5.2. Controlled movements of barrel MDT chambers

During the 2004 test beam period, several runs with controlled movements of all barrel MDTs were recorded. The aim of the study was to check the response of the alignment system *a)* in the presence of controlled chamber movements, and *b)* in conditions close to the dynamical range of the optical alignment sensors. Table 4 summarizes the range of these movements.
The reconstructed geometry was calculated using the *ASAP* software package; both alignment modes, relative and absolute, were tested. The reconstructed geometry in both modes was given as input to *Muonboy* and the sagitta for each event was calculated. The analysis criteria were the following: the event was accepted if it had only one reconstructed segment per barrel MDT chamber with at most one missing hit per segment. The sagitta for events satisfying these criteria was calculated with the two methods described in section 4.3.

Date	MDT chamber	Range of translations	Rotation around beam axis
July 2004	BIL (2^{nd} tower)	0 to 20 mm	(-8 , +8) mrad
November 2004	BIL (2^{nd} tower)	0 to 4.5 mm	(-3 , +2) mrad
	BML (2^{nd} tower)	0 to 4 mm	(-3 , +3) mrad
	BOL (2^{nd} tower)	0 to 6 mm	(0 , -2) mrad

Table 4: The range of barrel MDT movements during the 2004 test beam period.

In July 2004, three runs with barrel chamber movements were taken and data were recorded with a beam of pions triggered by a hodoscope. Figure 16 shows the sagitta distribution, after applying the absolute alignment corrections to the reconstructed segments. The sagitta residuals have a dispersion of 78 μm microns if one considers the absolute alignment corrections and 14 microns in the relative alignment mode (Figure 17).

In the November 2004 test beam period, 18 runs were recorded with controlled movements (translations and rotations) of all barrel MDT chambers. This time, a muon beam was used and the trigger area was 10cm x 10cm. The distribution of the sagitta, as calculated in the *ASAP* software package, is shown in Figure 18 as a function of the run number after applying the relative alignment corrections. One observes that, for some runs, the sagitta was several millimetres away from the mean value; these runs during which several optical sensors were out of range and did not work properly were not considered in the analysis.
In Figure 19, the distribution of the sagitta for seven runs is shown before and after applying the absolute alignment corrections. Before the alignment corrections are applied, the mean value of the sagitta is varying by several millimetres, which reflects the successive MDT chamber movements; once the alignment corrections are applied, all sagitta distributions are centered at the same mean value around zero, as expected. This analysis shows that, for the chamber movements during the November 2004 test beam period, the sagitta residuals have a dispersion of 63 μm (Figure 20) if one considers the absolute alignment corrections, and 18 μm for relative alignment.
It is worth noticing that the mean value of the sagitta, after applying the absolute alignment corrections, is of the order of 350 μm which is an indication of the level of control of these absolute corrections. Final calibrations of the optical alignment sensors will give us better results in the absolute mode, and will eventually lead to a mean value of the sagitta close to zero.

5.3. Summary of the alignment response of optical sensors

In sections 5.1 and 5.2 results on the alignment of MDT chambers using optical sensors in the H8 2004 test beam data were presented. Both alignment modes (relative and absolute) were studied.
In the relative mode, both barrel and end-cap results show that the precision is of the order of 20 μm. For the absolute mode, which was tested for the first time in 2004, the mean value of the sagitta is known with a 350 μm uncertainty in the barrel and 150 μm in the end-cap. We expect the remaining shift from zero (the theoretical sagitta value for straight tracks!) to be reduced significantly once the final calibration of the optical alignment sensors is available. Nevertheless, these results must be considered as a complete success in understanding the relative alignment mode and very encouraging for the absolute alignment mode.

6. Results on alignment with tracks

An essential part of the alignment of the ATLAS muon spectrometer consists in using tracks for inferring constraints on chamber positions. This will be done both during commissioning runs, and during physics runs. As an exercise to check the feasibility of the alignment using real data, we have set up and tested the tools to perform alignment with straight tracks on several H8 runs.
An ATLAS note has been released describing in great details the outcome of this analysis **[10]**. Here only a summary of this analysis will be presented.

6.1. Alignment strategy: principle of the method

A track may be seen as a sample of hits, associated together by a pattern recognition algorithm. A χ^2 function may be built for each track, which will depend on track parameters, and on the spatial coordinates and orientation of the sensitive devices producing the hits:

$$\chi^2_{\text{track i}}(a, p_i) = \sum_{\text{hits j}} \chi^2_{\text{hit i,j}}(a, p_i) \quad (2)$$

In the previous expression, *i* denotes the track index, and *j* the hit index of track *i*. The vector **a** represents the complete set of chamber position parameters, and $\boldsymbol{p}_i$ the four straight-track parameters.
Track fitting consists in finding the best set of parameters $\boldsymbol{p}_i$ for a given alignment **a**:

$$\hat{\chi}^2_{\text{track i}}(\alpha) = \min_{p_i}\left(\chi^2_{\text{track i}}(\alpha, p_i)\right) \quad (3)$$

In other words, the value of the χ^2 at the minimum depends on the alignment considered.
Given a sample of tracks, the alignment may be estimated by minimizing the following function:

$$\chi^2_{\text{align}}(\alpha) = \sum_{\text{tracks i}} \hat{\chi}^2_{\text{track i}}(\alpha) \quad (4)$$

In practice, the sample of tracks in H8 consists of several thousands of tracks, and of the order of 15 chamber parameters are fitted using MINUIT. The total χ^2 function is called several hundreds of times in this operation, and each time it is called, each track needs to be refitted.

6.2. Alignment dedicated tracking tools

The following tools have thus been developed to perform alignment on H8 runs:

- a fast straight track fitter,
- a rough T0 and RT calibrator,
- a pattern recognition algorithm.

Details on motivations, performance and resolution of these tools may be found in **[10]**.

6.3. H8 beam conditions, fitted parameters

For performing track-based alignment, it is essential to illuminate the largest possible portion of the chambers with the beam. Given this requirement, we concentrate only on the runs recorded using the hodoscope trigger. However, tracks from hodoscope samples are parallel at the level of 5 mrad, and also, the illuminated portion of the chambers, even with the hodoscope runs, is very small. This implies that some degrees of freedom may not be fitted at H8. The list of parameters that may be fitted is illustrated in Figure 21.

6.4. Results and validations

The result of the alignment fit is presented in Figure 22. The alignment obtained using the track is consistent with the survey positions and with the movements of the chambers that were made between the period of the survey and the period of the recording of the run.
Figure 23 and Figure 24 show the sagitta of the selected tracks, before and after the alignment fit. The mean value of the sagitta is completely corrected within 5 μm, and the width is also improved.
Figure 25 and Figure 26 show the variation of the sagitta as a function of chamber coordinates. The alignment procedure corrects these residuals.

6.5. Systematic error

A procedure has been set up to compare the track-based alignment with the optical relative alignment (explanations on this procedure can be found in **[10]**).
The procedure to do this is illustrated in Figure 27. The starting point is a pair of runs, between which some movements of the chambers have been performed. Track-based alignment is performed on these two runs: let's call the corresponding alignment corrections A1 and A2. The first set of correction A1 is then used as reference geometry for ASAP in relative mode, which can in turn extrapolate the geometry to the period of the second run by using the response of the optical sensors only. Let's call this extrapolated alignment A'2. If every correction is perfect, then we should find that A2 and A'2 are the same. If they are not the same, then we attribute the error to the track-based alignment procedure, because we have great trust in the optical relative alignment: its reliability has been proved many times at the test beam.
Figure 28 and Figure 29 show the impact on sagitta of reconstructed tracks of alignments A2 and A'2, where large movements of the chambers had been performed in the initial pair of runs (BIL chambers were rotated by 6 mrad around beam axis). The two alignments present the same small bias on the sagitta (30 μm), within 7 μm. The track-based alignment is thus believed to be very precise in the degrees of freedom to which H8 tracks are sensitive. A further test is presented in **[10],** which shows that, including the other degrees of freedom, the precision of the track-based alignment is a few hundred microns. This last feature is expected to vanish when we will use cosmic data with a large angular spread of the tracks.

7. Segment and track reconstruction studies

7.1. Track segment efficiency

The aim of this study was to measure the track segment and single hit efficiencies of the MDT chambers and to check the stability of the results in various operational conditions. For these studies, runs recorded with the 10x10 cm trigger setup and a number of H8 beam energies and MDT operational thresholds, were analyzed. In the 2004 H8 setup, the beam was crossing the boundary area between the two towers of BML, which was a source of large inefficiencies. In order to avoid these inefficiencies in this particular study, we used runs in which the beam was deflected horizontally by the BMPL magnet in such a way as to cross mostly the chamber of tower 2.
In order to calculate the track segment efficiency of one MDT chamber (barrel or end-cap) the following method was developed. Two of the three stations (barrel or end-

cap) belonging to the same tower, are chosen as reference stations (a schematic view of the method is shown in Figure 30). In each reference station, we request no more than one reconstructed segment, with a total number of hits of at least (max-1), where max is the number of tube layers in a chamber. For example, the minimum number of hits should be 7 in BIL chambers and 5 in BML or BOL chambers. Our reference sample contains events, which satisfy these conditions.
With the two reconstructed segments of the reference stations, the sagitta is calculated for all the reconstructed segments of the tested station, as explained in 4.3. The distribution of the sagitta is plotted and a number of areas are defined, centred on the mean value of the sagitta distribution and with increasing widths n*σ (Figure 31). The good segments with the correct minimum number of hits are counted in each area.
The ratio of good segments to the reference sample is calculated and plotted as a function of the distance from the mean value (Figure 32). A plateau is reached after 3 σ. A linear fit of the plateau provides the track segment efficiency through the fit parameter.
This method is applied to both the barrel and end-cap chambers and the results are presented in Table 5.

Track segment efficiency (%)			
N_{hits}	**BIL**	**BML**	**BOL**
≥ MAX-1	93.2 ± 0.2	94.3 ± 0.1	96.3 ± 0.2
= MAX	68.2 ± 0.3	71.5 ± 0.3	76.3 ± 0.4

N_{hits}	**EIL**	**EML**	**EOL**
≥ MAX-1	89.8 ± 0.2	94.9 ± 0.2	95.3 ± 0.1
= MAX	63.7 ± 0.3	74.4 ± 0.4	75. 6 ± 0.2

Table 5: Track segment efficiency (%), for different number of hits, for barrel and end-cap chambers.

7.1.1. Track segment efficiency as a function of beam energy and MDT threshold

In order to investigate the dependence of track segment efficiency on the energy of the muons, runs for different beam energies have been analyzed. Figure 33 a) shows the track segment efficiency as a function of beam energy, for the nominal MDT threshold (-40mV) of the BOL chamber. As expected, the track segment efficiency is independent of the beam energy.
The track segment efficiency was also studied for various MDT thresholds, and results for the EOL chamber are presented in Figure 33 b). The track segment efficiency is stable for thresholds above the nominal -40 mV threshold and drops by ~2% for the lower threshold (-36mV). This efficiency drop is due to the increased noise when the MDT threshold is lowered.

7.1.2. Single hit efficiency

The single hit efficiency (ε_{hit}) can be extracted from the track segment efficiency. Let n_{hits} be the minimum number of required hits and n_{total} the total number of hits in a segment; then the track segment efficiency is related to the single hit efficiency through:

$$\varepsilon(n_{hits}/n_{total}) = \frac{n_{total}!}{n_{hits}!(n_{total}-n_{hits})!}(\varepsilon_{hit})^{n_{hits}} \cdot (1-\varepsilon_{hit})^{(n_{total}-n_{hits})} \qquad (5)$$

Table 6 shows single hit efficiencies, extracted from the track segment efficiencies, for barrel and end-cap chambers and for two cases: $n_{hits} = n_{total}$ and $n_{hits} = n_{total}$ -1. We observe that similar single hit efficiencies are found for both the barrel and end-cap chambers, as expected.

Single hit efficiency (%)

N_{hits}	BIL	BML	BOL
n_{total}-1	95.8 ± 0.1	95.1 ± 0.2	95.9 ± 0.2
n_{total}	95.3 ± 0.1	94.6 ± 0.1	95.6 ± 0.1

N_{hits}	EIL	EML	EOL
= n_{total}-1	95.5 ± 0.1	95.8 ± 0.2	95.9 ± 0.2
= n_{total}	94.5 ± 0.1	95.2 ± 0.1	95.4 ± 0.1

Table 6: Single hit efficiencies (%) of the barrel and end-cap chambers

7.1.3. Effect of material in front of the chambers

For some runs of the last running period (November 2004), a 15x15x1 cm^3 block of stainless steel was placed in the beam path in front of all barrel chambers, BIL, BML and BOL,(a picture of which is shown in Figure 34), in order to study the effect of this material on the performance of the pattern recognition algorithm. The effect of added material on the track segment efficiency and the single hit efficiency was studied only for the BOL chamber because of the following reasons:

a) the MBPL magnet to deflect the beam was not available, therefore the beam was crossing the area between the two BML chambers and
b) in the case of BIL chambers, one tube in the beam sensitive area was not working ; the beam profile of the BIL chamber is shown in Figure 35.

Table 7 shows the track segment efficiency and single hit efficiency for two runs, one with the presence of material and one without material in front of the BOL chamber. One observes a 1% drop of the single hit efficiency in the presence of material.

Track segment efficiency (%) of BOL for 180 GeV muons		
	Without material	**With material**
$N_{hits} \geq$ **max-1**	93.5 ± 0.3	91.7 ± 0.4
N_{hits}**= max**	70.1 ± 0.7	66.1 ± 0.6

Single hit efficiency (%) of BOL for 180 GeV muons		
	Without material	**With material**
$N_{hits} = n_{total}$**-1**	94.9 ± 0.2	94.3 ± 0.2
$N_{hits} = n_{total}$	94.3 ± 0.1	93.3 ± 0.2

Table 7: Track and single hit efficiencies in the BOL chamber in the presence of material for 180 GeV muons**.**

7.2. Tracking and backtracking

7.2.1. Tracking muons in the magnetic field

The MBPS magnet was installed between the EI and EM stations of the end-cap setup to perform muon momentum measurements. This magnet was located at x= 45.3 m and operated with several current settings and the two orientations of the magnetic field. Figure 36 shows the variation of the main B-field component along the y-axis for a current value of 800 A, as a function of the position along the beam axis (x). The field at the center of the magnet is 2 Tesla.
Only pion runs are available for this study. For pion beam energy of 350 GeV, one expects mean muon energy of ~180 GeV. The magnetic field map was used to measure muon deflection.
Requiring the track to be reconstructed in all 6 MDT (barrel +end-cap) chambers and after applying cuts on the second coordinate measurement, the mean value of the momentum distribution is 150 GeV. This result is encouraging, but a better knowledge of beam properties is required to make a more quantitative statement. The result of tracking in the magnetic field is illustrated in Figure 37.

7.2.2. Backtracking to the perigee

An additional improvement of the reconstruction, made possible by the accurate description of material, deals with energy losses in the calorimeters and the iron dump as well as in the muon system itself. Although energy losses and their distribution along the muon track have a very small impact on muon reconstruction inside the muon system, they play an important role in backtracking the reconstructed muon to the perigee (x=0). During this backtracking, the muon momentum is corrected only for the average energy loss which is estimated from the reconstructed momentum as well as from the amount and nature of the material traversed by the reconstructed muon trajectory.

A detailed geometry description of the H8 setup is provided by AMDB. The momentum correction for energy loss in materials is made in *Muonboy*; contributions come from magnets (MBPL and MBPS), the iron dump, and the calorimeters (Tile and liquid argon). The effects of multiple scattering and energy loss fluctuations are taken into account in the covariance matrix propagation given by *Muonboy***.**
Reconstructed track parameters with their full covariance matrices are provided at the entrance of the muon spectrometer, at the entrance of the calorimeters and at the perigee of the track.
The distribution of the z coordinate of the muon tracks extrapolated from the muon spectrometer (MS) to the perigee is shown in
Figure 38. The most populated region of this distribution lies between -70mm and +70mm, which correspond to the MBPSID aperture. This demonstrates that the backtracking is working correctly.
The impact parameter at the perigee, shown in
Figure 39, has a mean value of (20.3 + 0.6) mm. This result shows that the extrapolation from the muon spectrometer to the perigee over a distance of ~ 40 m works very well.

7.2.3. Inner detector and muon spectrometer correlations

With the combined test beam data it is possible to correlate measurements made in the muon spectrometer with those made in other detectors of the setup. The track reconstruction in the inner detector (ID) is performed by the *StraightLineFitter* package and the track reconstruction in the muon system is performed using *Muonboy*. The track correlation is evaluated at the perigee.
The correlations in the z coordinate (precision coordinate) shown in Figure 40 is excellent, as the slope is compatible with 1.The -7.9 mm offset represents the small misalignment of the inner detector with respect to the muon system.

7.2.4. Aligning the Inner Detector with the Muon spectrometer

A first attempt to align the inner detector with the muon system is made by using the concept of *alignment with tracks* described in section 6. The method relies on minimizing a χ^2 based on the variables describing the distance and angles between the inner detector and the muon system. In this procedure, the inner detector is allowed to move relative to the fixed position of the muon system.
The correlation between the inner detector and the muon system after alignment is shown in Figure 41; the residual shift between the two detectors, (0.31 ± 0.68) mm, signals a very good alignment within the experimental uncertainty.

8. Conclusions

In this note we present a variety of results obtained with the Muon Spectrometer stand in the ATLAS combined test-beam setup of 2004.

A prototype of the full ATLAS offline reconstruction was tested successfully.

The results on the alignment of the MDT chambers provided very valuable information in the following domains:

i) The optical alignment system was tested and validated in both the barrel and end-cap systems.
ii) Both alignment modes (*absolut*e and *relative)* were studied and tested; the results are within the specifications. For the first time the absolute mode was tested with the barrel alignment system with very encouraging results.
iii) For the first time the concept of the alignment using real data has been tested and validated using straight tracks from the H8 data.

The studies of MDT chamber efficiencies, with different beam energies, MDT thresholds, and in the presence of material in front of the chambers, showed very stable results as expected.

Finally the studies on the tracking in the Muon Spectrometer stand and the backtracking up to the Inner Detector, showed the good efficiency and robustness of the muon reconstruction program *Muonboy*. A first attempt of relative alignment of the Inner Detector with the Muon Spectrometer was also performed with the H8 data.

Acknowledgements
The collection of the test beam data represents a joint effort of many individuals in the ATLAS collaboration. We would like to thank them for their contributions.

References

[1] "The ATLAS Muon Spectrometer Technical Design Report, The ATLAS Muon Collaboration", CERN/LHCC/97-22, 31 May 1997.

[2] "Beamline instrumentation in the 2004 combined ATLAS testbeam", B. Di Girolamo et al., ATL-TECH-PUB-2005-001.

[3] "First system performance experience with the ATLAS high-precision muon drift tube chambers", H. van der Graaf et al., Nucl. Instr. And Meth. In Phys Res A419 (1998) 336.

[4] "The BCAM Camera" K. Hashemi, J.Bensinger , ATL-MUON-2000-024.

[5] "The alignment system of the ATLAS Muon Spectrometer", Ch. Amelung et al., Eur. Phys. J. C33, s01 (2004) 999.

[6] ASAP home page: http://florian.home.cern.ch/florian/Asap.html

[7] ARAMYS home page: http://amelung.home.cern.ch/amelung/aramys.html

[8] "Study of MDT calibration constants using H8 testbeam data of year 2004" Baroncelli T. et al., ATL-COM-MUON-2006-015, 05-Jul-2006.

[9] "The AMDB documentation", Saclay Muon Group, available at http://muondoc.web.cern.ch/muondoc/Software/DetectorDescription/amdbdoc/amdbmanual.ps

[10] "Track based absolute alignment in the ATLAS Muon Spectrometer and in the H8 test beam" P.F.Giraud et al., ATL-MUON-PUB-2006-012.

[11]"The PERSINT Manual" Virchaux M.; Pomarede D., ATL-SOFT-2001-003, 31-Jan-2001; https://uimon.cern.ch/twiki/bin/view/Atlas/PersintWiki

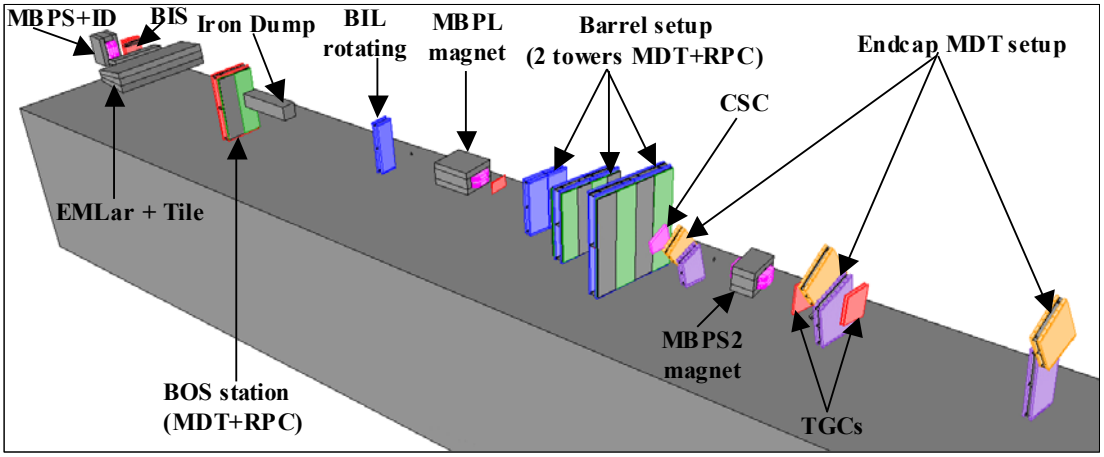

Figure 1: View of the H8 combined test beam setup of 2004, made with the PERSINT **[11]** graphics tool.

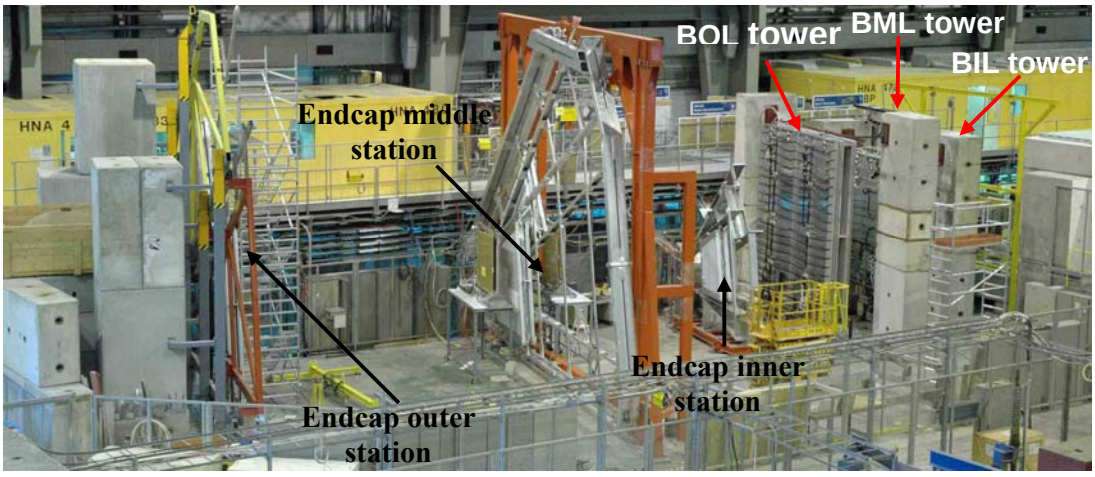

Figure 2: View of the H8 muon system experimental setup.

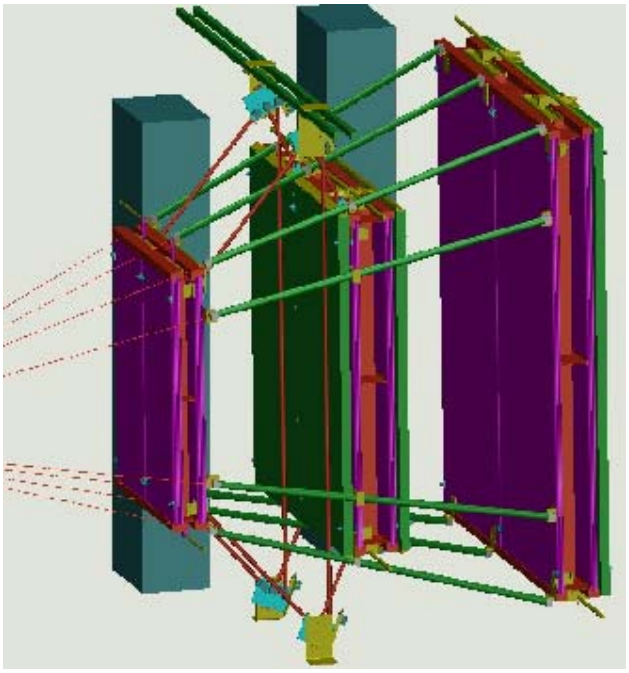

Figure 3: Schematic view of the barrel alignment system of H8. The projective (green) and the reference (red) lines are visible.

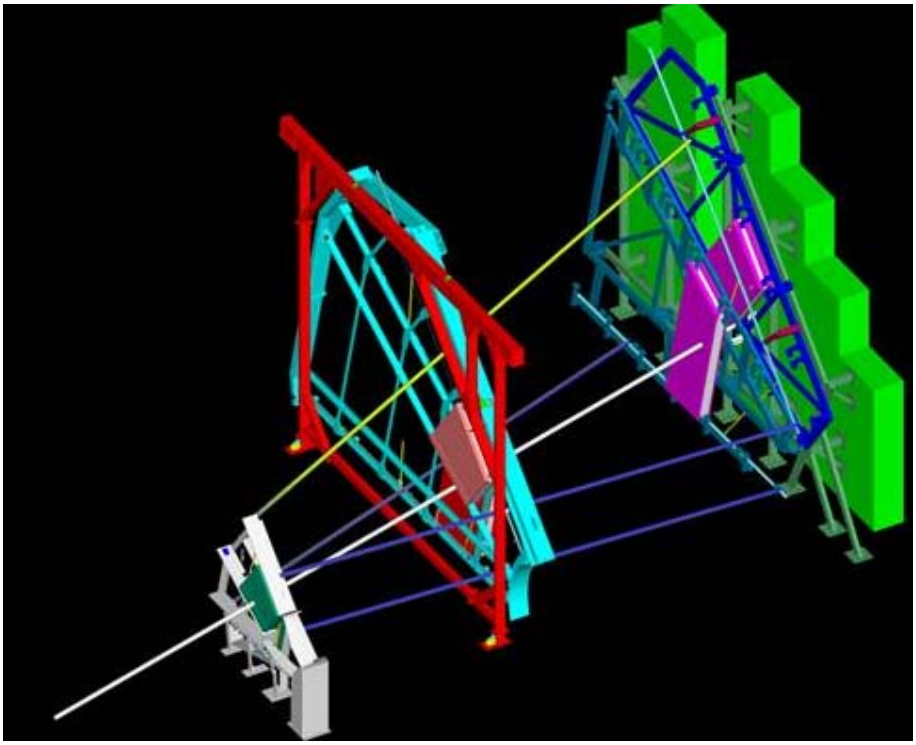

Figure 4: Schematic view of the end-cap alignment system of H8.

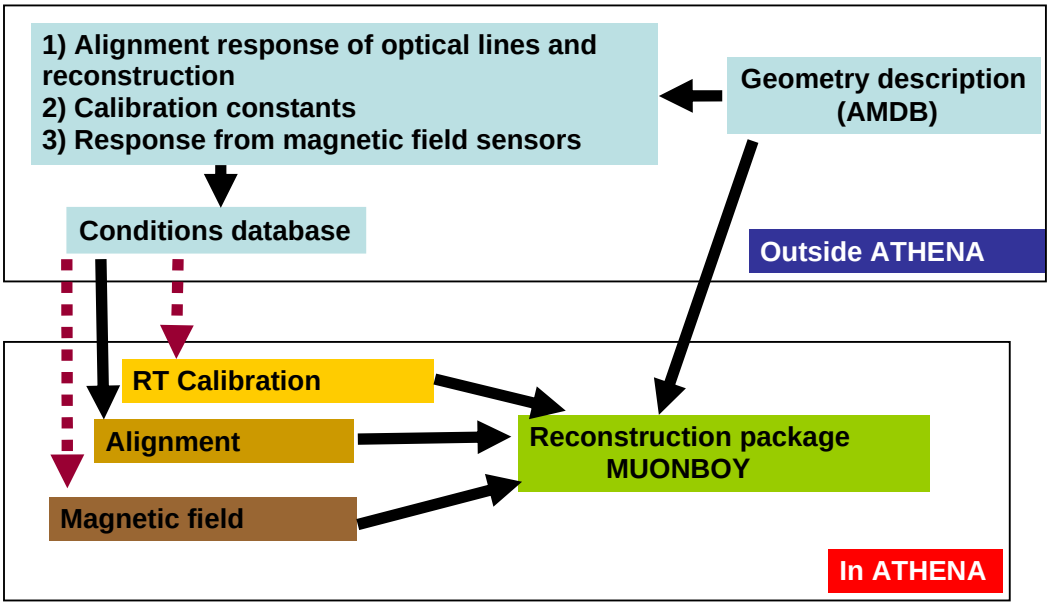

Figure 5: ATLAS scheme for muon offline reconstruction. The dotted lines show parts in this scheme that were not implemented in the H8 data flow.

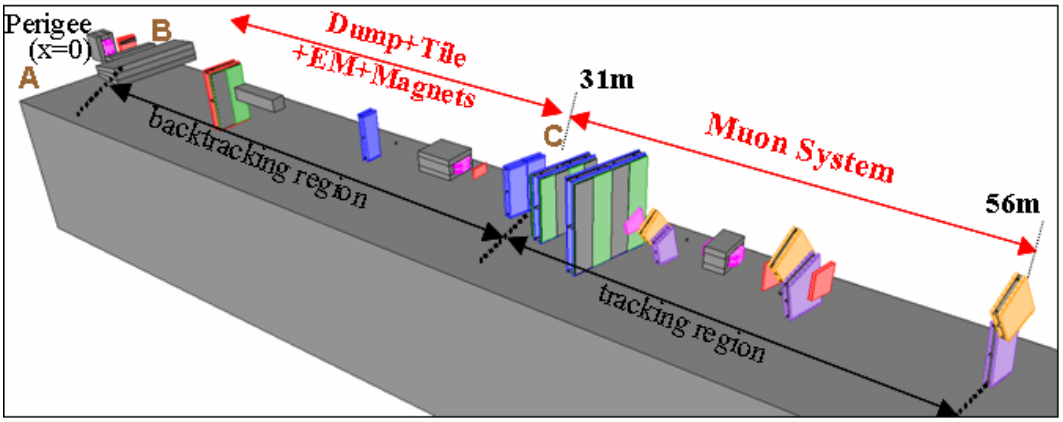

Figure 6: Schematic view of the H8 setup. The three locations where the reconstructed track parameters and their full covariance matrices are provided by the *Muonboy* reconstruction package are (A) at the perigee point (x=0), (B) at the entrance of the calorimeters and (C) at the entrance of the muon spectrometer (here at 31 m).

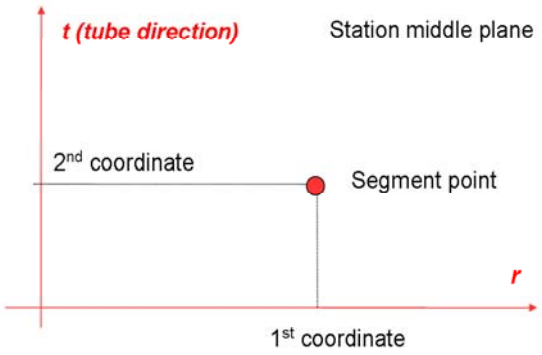

Figure 7: Definition of 1st and 2nd coordinates in the middle plane of a station.

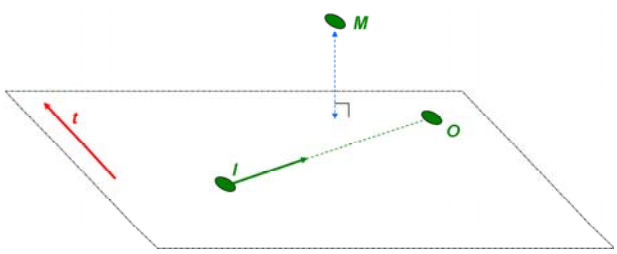

Figure 8: Definition of the sagitta.

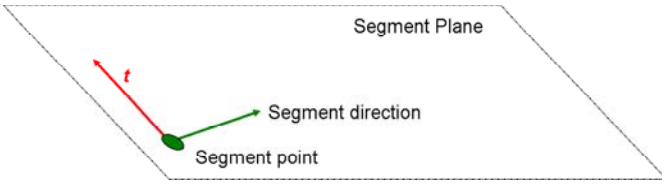

Figure 9: Definition of a segment plane.

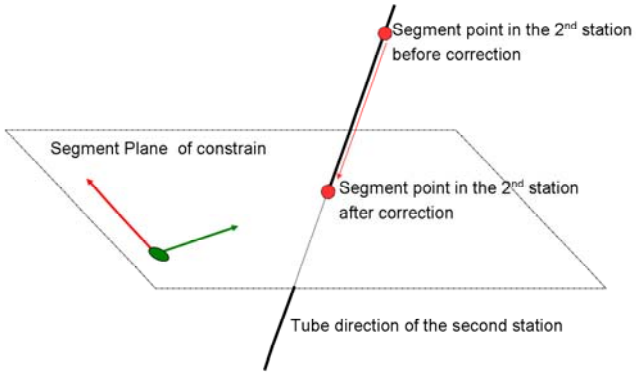

Figure 10: Principle of the method for determining the second coordinate from MDT measurements.

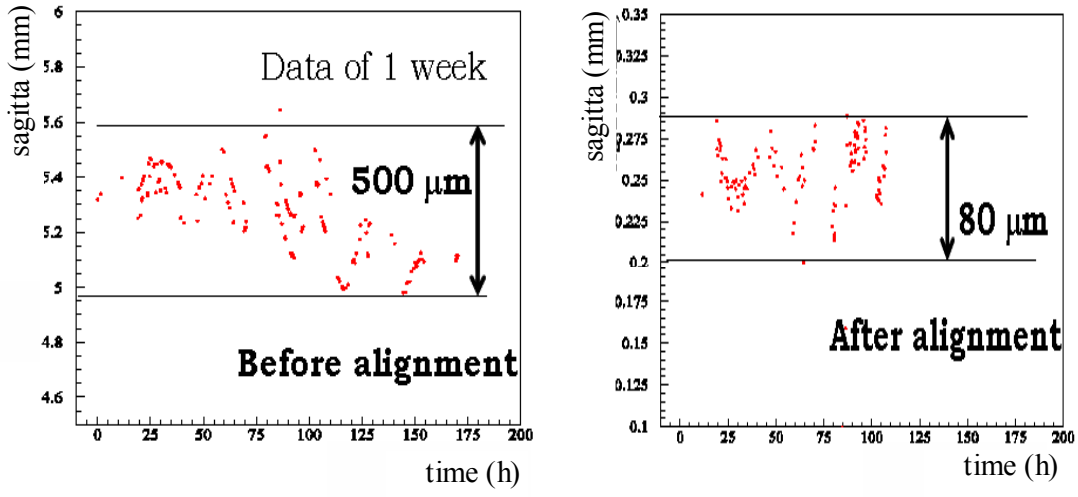

Figure 11: Left (right) plot: variation of the *sagitta* as a function of time in the end-cap before (after) applying the alignment corrections.

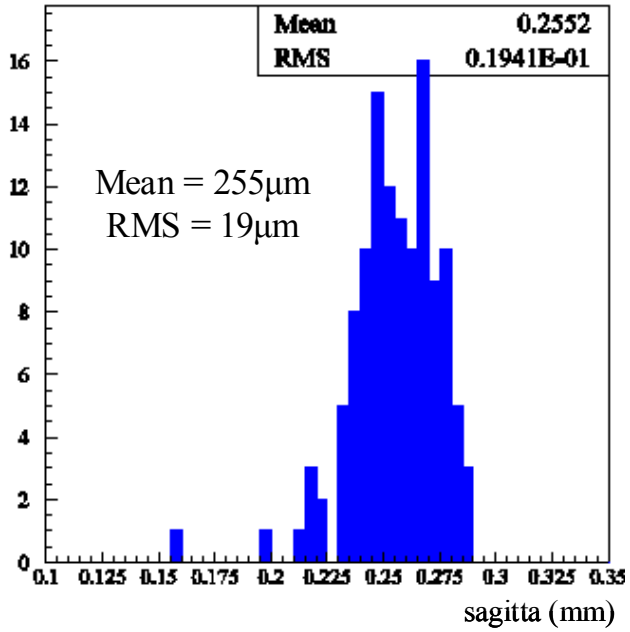

Figure 12: Mean values of the *sagitta* in the end-cap, calculated after applying the alignment corrections, for various runs recorded in a one week period.

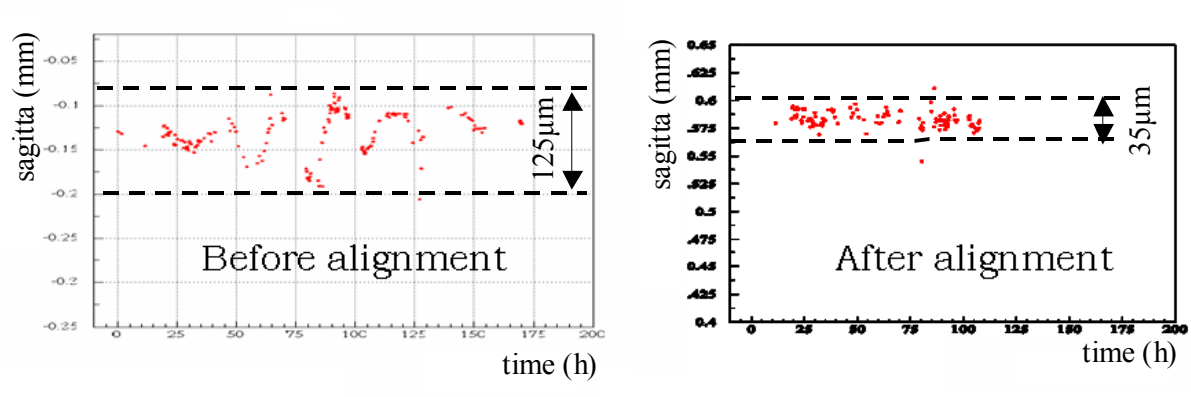

Figure 13: Left (right) plot: *sagitta* variations as a function of time in the barrel before (after) applying the relative alignment corrections.

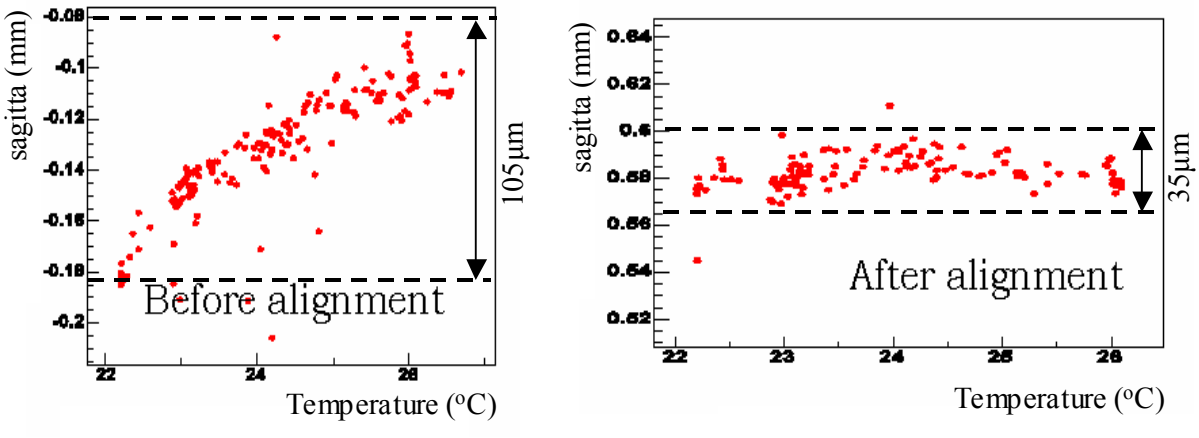

Figure 14 Left (right) plot: *sagitta* variations as a function of temperature in the barrel before (after) applying the relative alignment corrections.

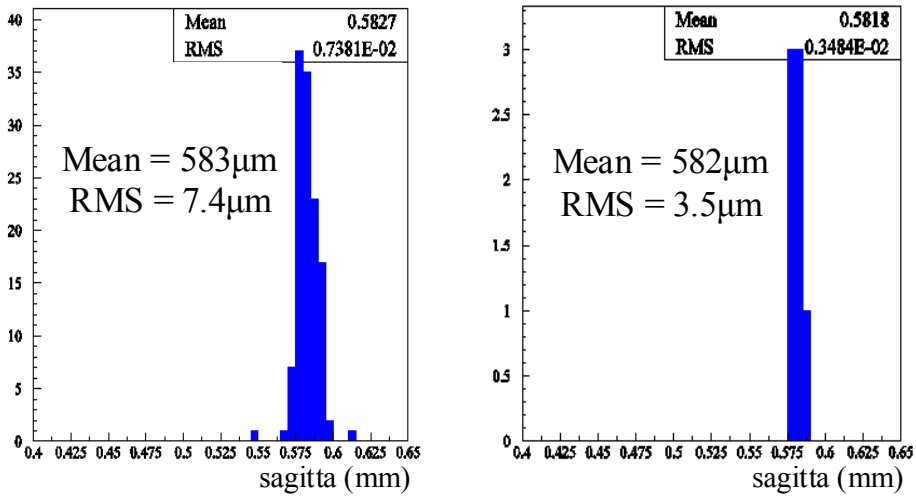

Figure 15: Left plot: mean value of the *sagitta* in the barrel for a one week data period. Right plot: mean value of the *sagitta* for some runs recorded one month later. The mean value is stable within a few µm.

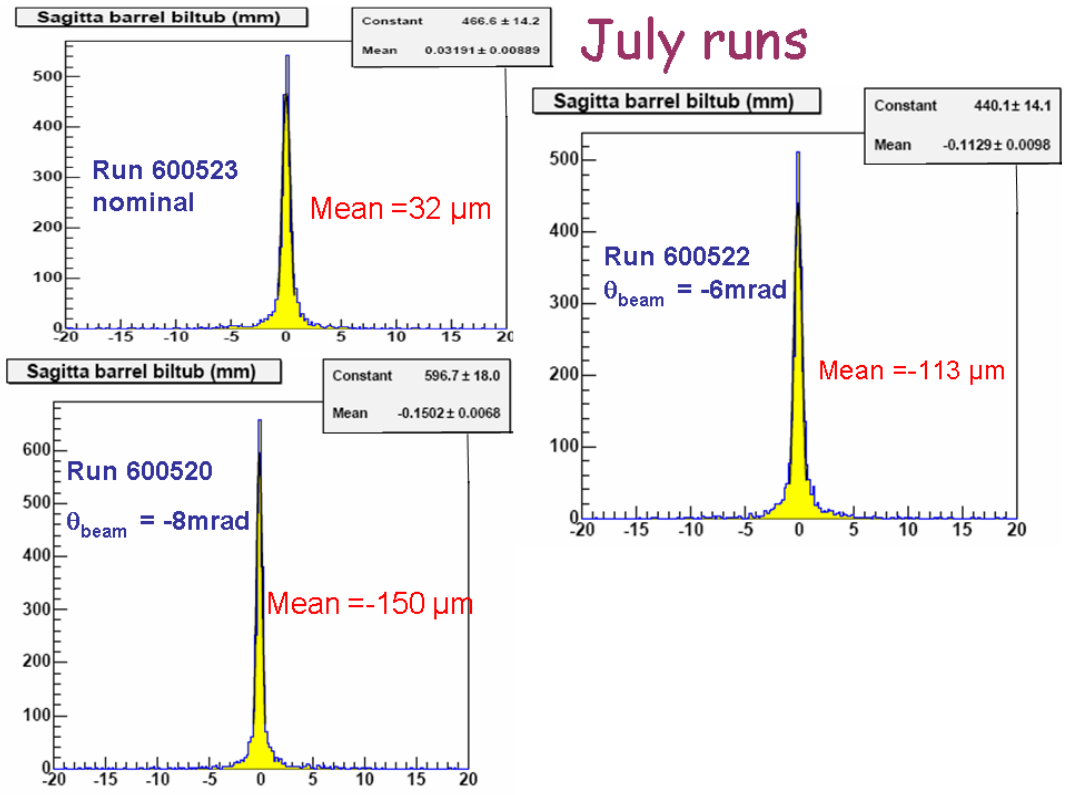

Figure 16: Distribution of the *sagitta* for three runs in which controlled movements of barrel MDT chambers were recorded. The absolute alignment corrections from the ASAP software package were taken into account in the *Muonboy* package to reconstruct the track segments for the *sagitta* calculation.

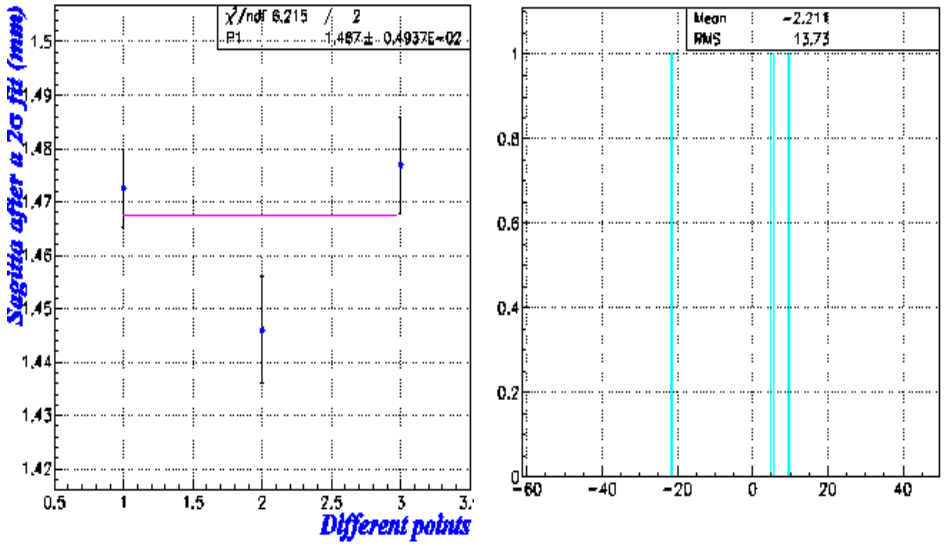

Figure 17: Residuals of *sagitta* for the three runs of the July 2004 period, during which controlled movements of barrel MDT chambers were recorded. In this figure, relative alignment corrections coming from the ASAP package are shown.

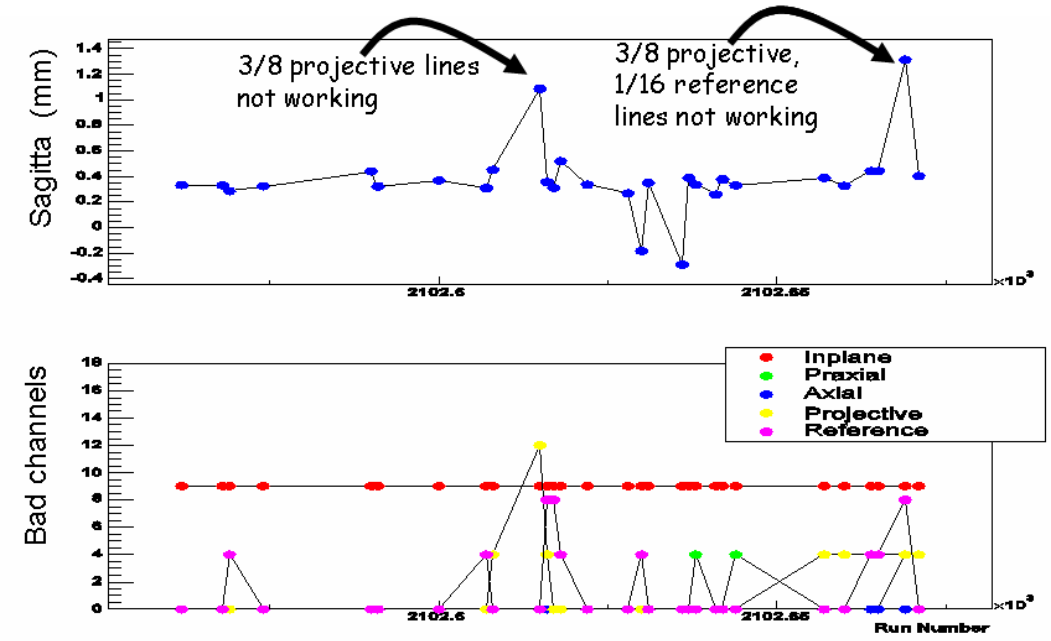

Figure 18: Upper plot: Distribution of the *sagitta* after applying relative alignment corrections as a function of the run number. For runs in which several optical lines were not functioning correctly the variation of the *sagitta* from the mean value is several millimeters. Lower plot: number of barrel alignment optical lines that were not working properly, as a function of the run number.

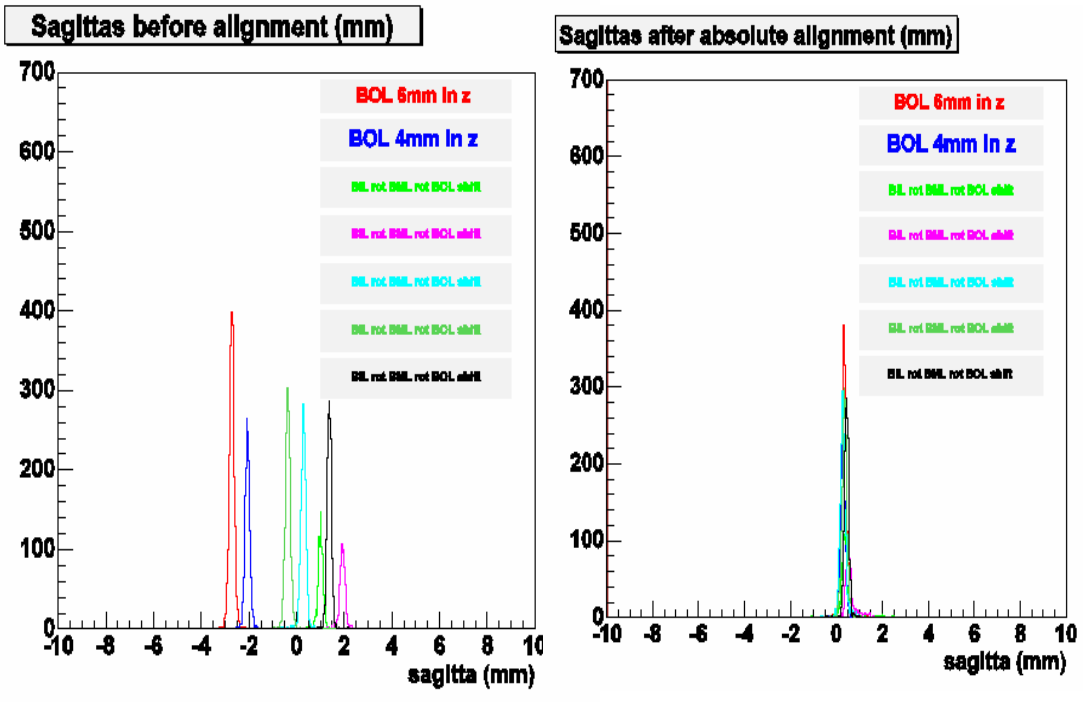

Figure 19: Left plot: the *sagitta* distribution for 7 runs in which different controlled movements of MDT chambers were performed, before alignment corrections. Right plot: *sagitta* distribution for the same runs, after applying the absolute alignment corrections.

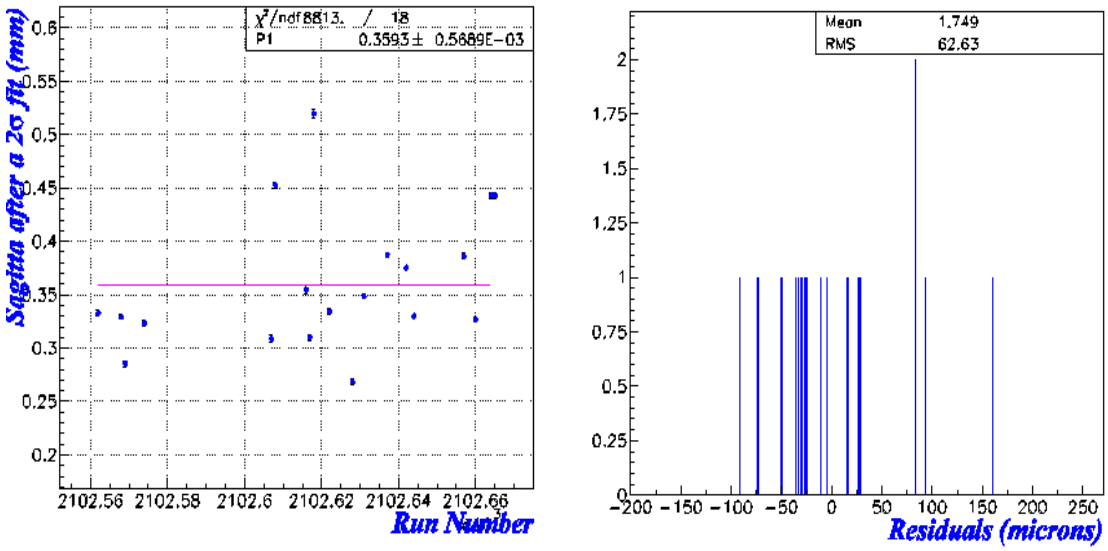

Figure 20: *Sagitta* residuals for the 18 runs of controlled movements of all barrel MDT chambers, after applying the absolute alignment corrections. The dispersion is of the order of 63 μm.

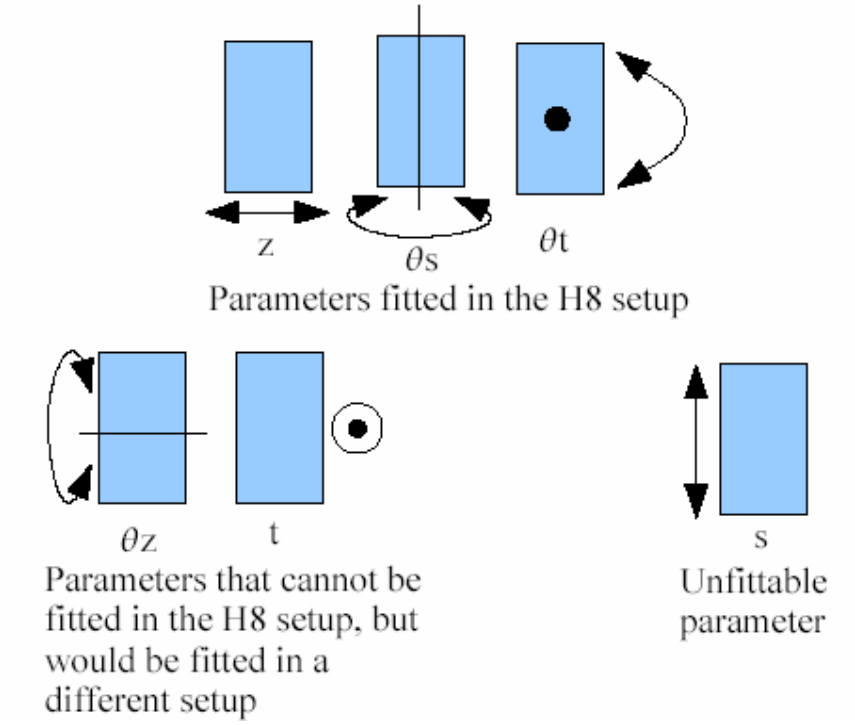

Figure 21: Illustration of the parameters that may be fitted for the alignment of the chambers in the H8 setup. The tube direction is s.

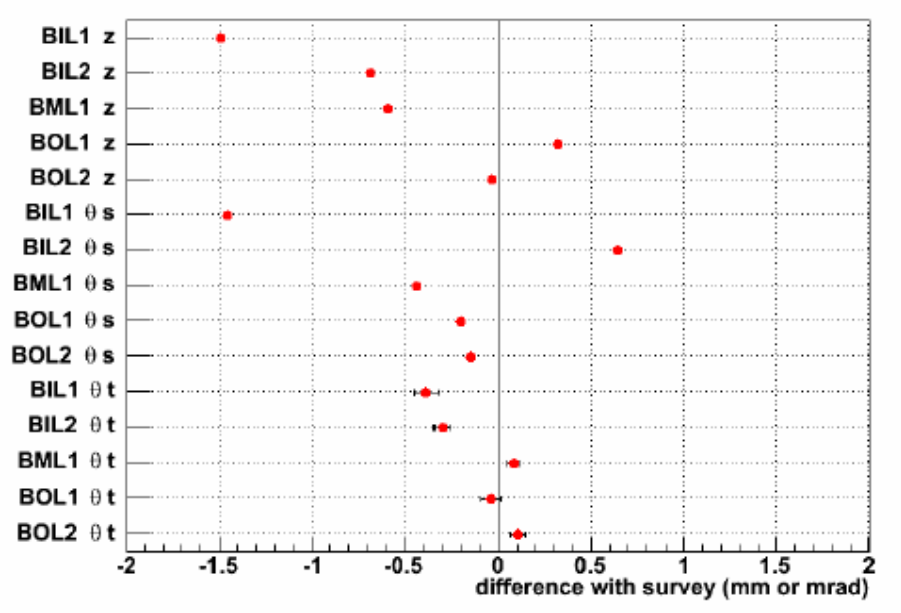

Figure 22: Results of the alignment fit. The reference for the fitted parameters is taken at the survey position.

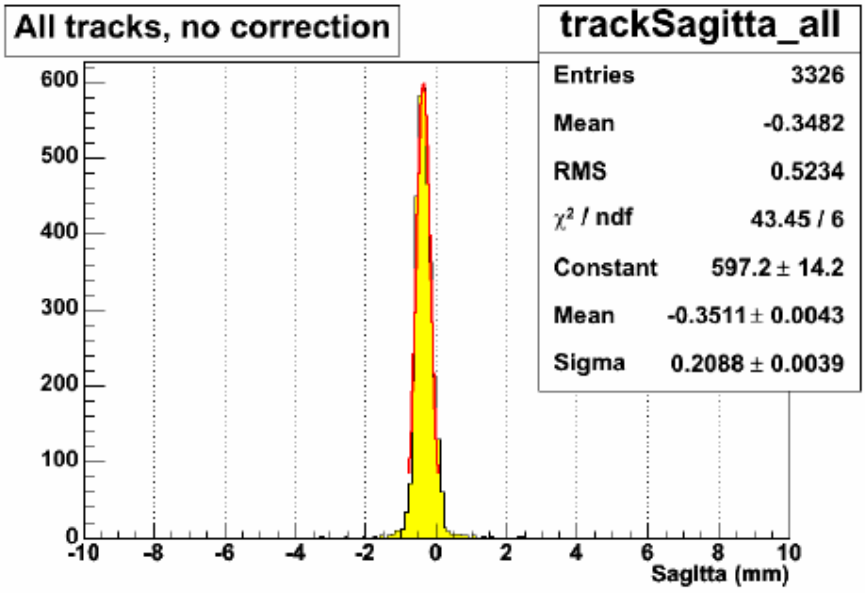

Figure 23: Sagitta of the selected tracks with the chambers at the survey position. The muon sagitta is centered at about –350 μm.

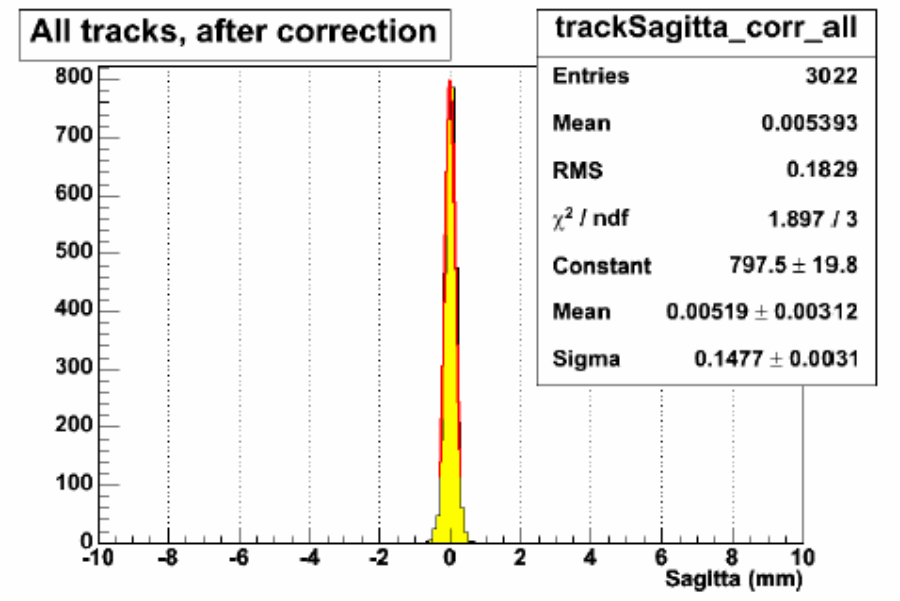

Figure 24: Sagitta of the selected tracks after alignment fit. The mean value of sagitta is now about 5 μm.

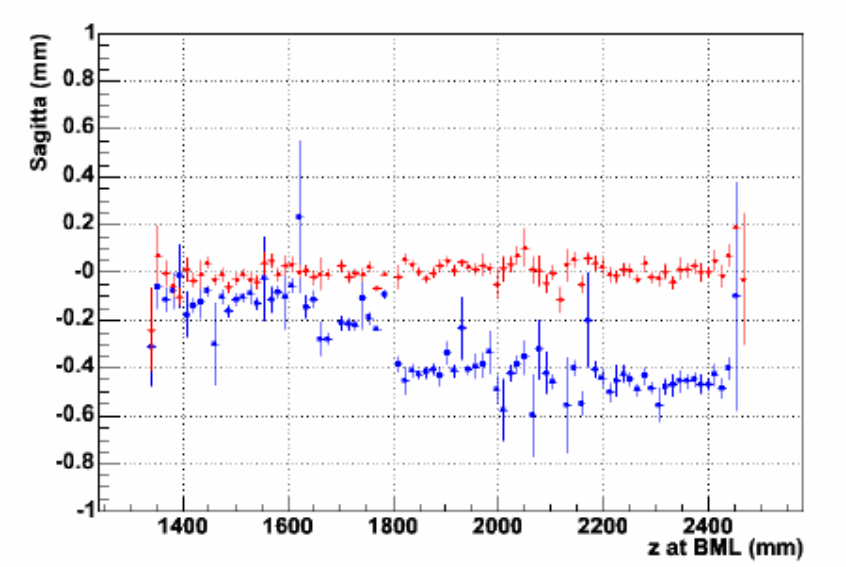

Figure 25: Mean value of the sagitta as a function of the BML chamber coordinates. In blue(dark) before correction and in red(light) after correction. z=1800mm is the location of the transition between BML1 and BML2.

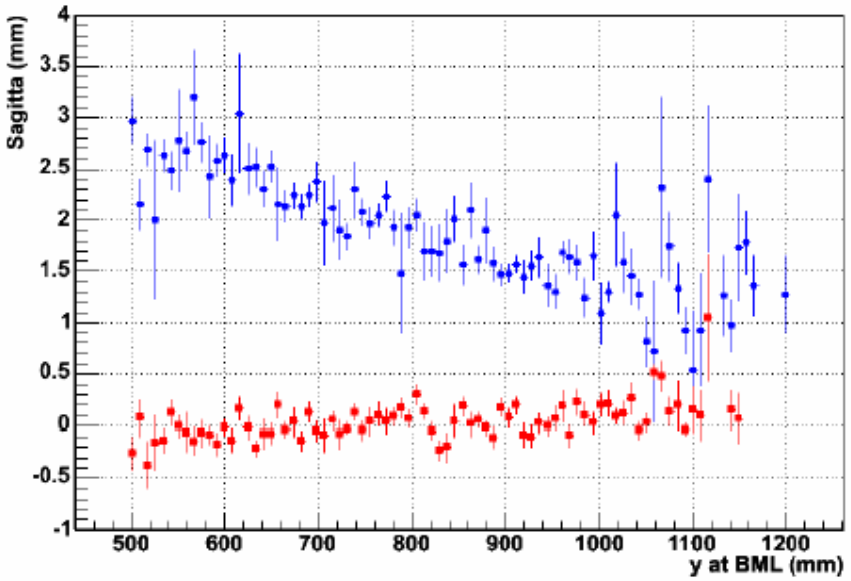

Figure 26: Mean value of the sagitta as a function of the second coordinate seen at the BML for run 600522 (large displacement of the chambers). In blue (dark) before correction and in red (light) after correction.

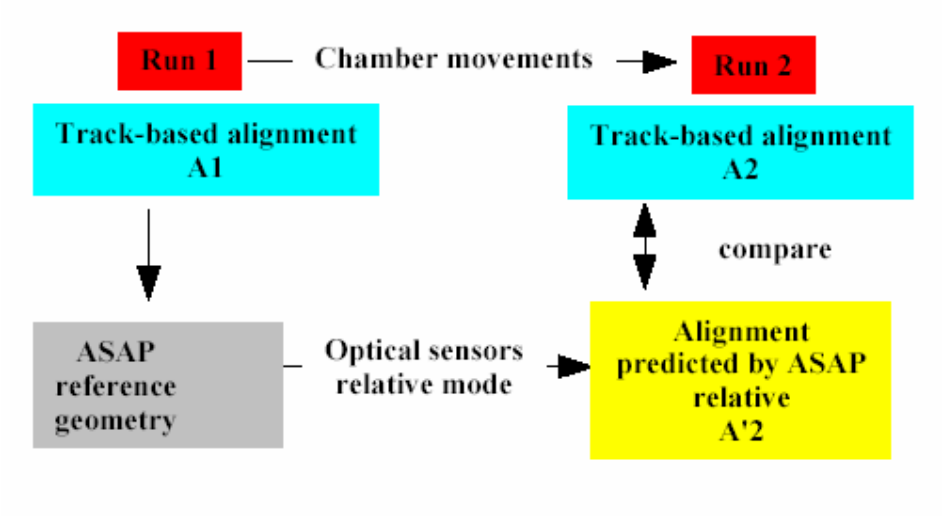

Figure 27: Illustration of the procedure for estimating the systematic error on track based alignment, using the optical alignment.

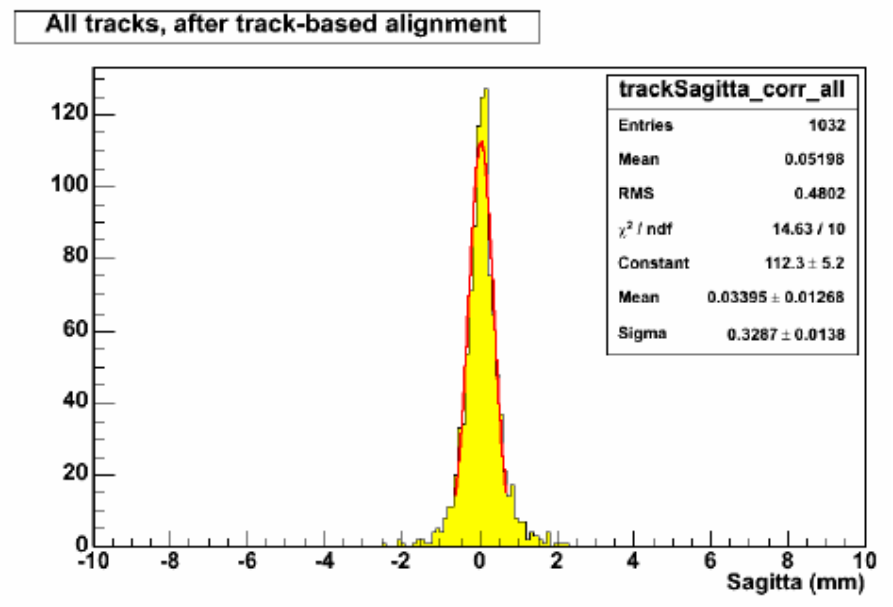

Figure 28: Sagitta of the tracks in a run where BIL chambers were rotated by 6 mrad around the beam direction, after track-based alignment corrections. (Alignment A2 in the text)

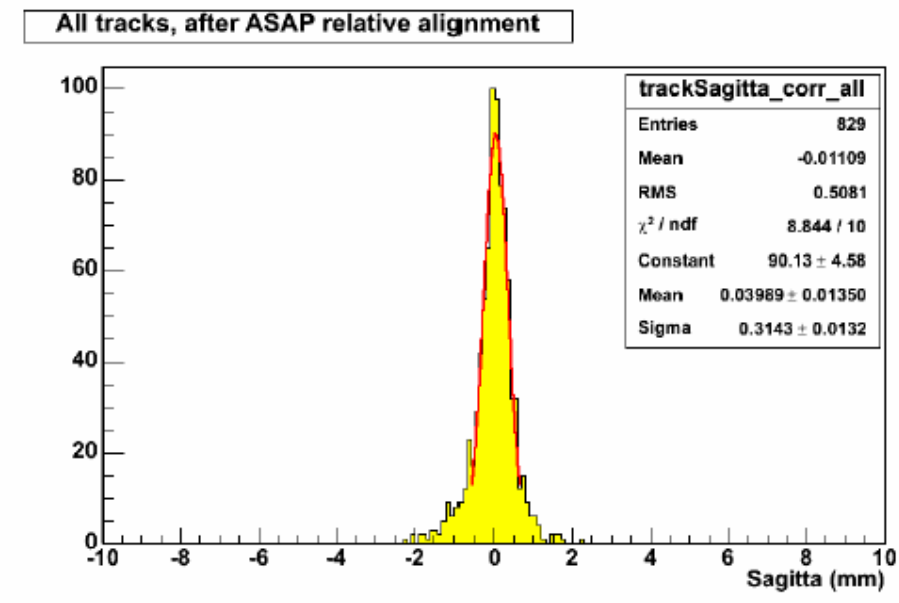

Figure 29: Sagitta of the tracks in the same run as Figure 28. Here track-based alignment is performed on a run where the chambers are in the nominal position, and ASAP in relative mode is used to extrapolate the alignment to the time of the plot. (Alignment A´ 2 in the text)

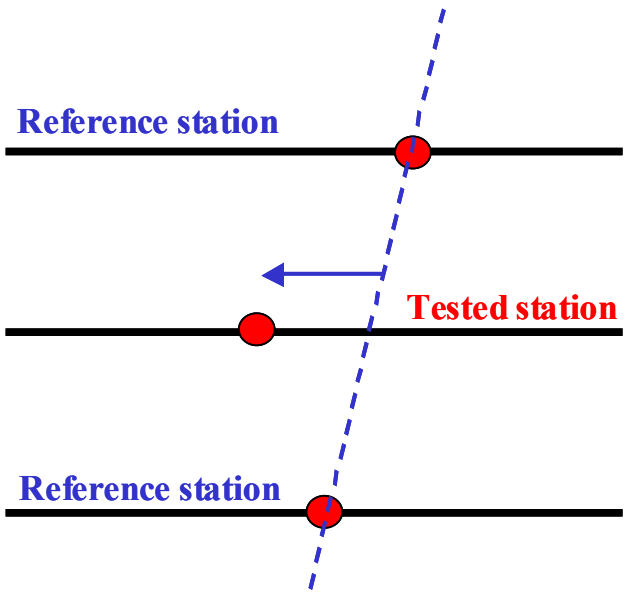

Figure 30: Schematic view of the method used for the calculation of the track segment efficiency.

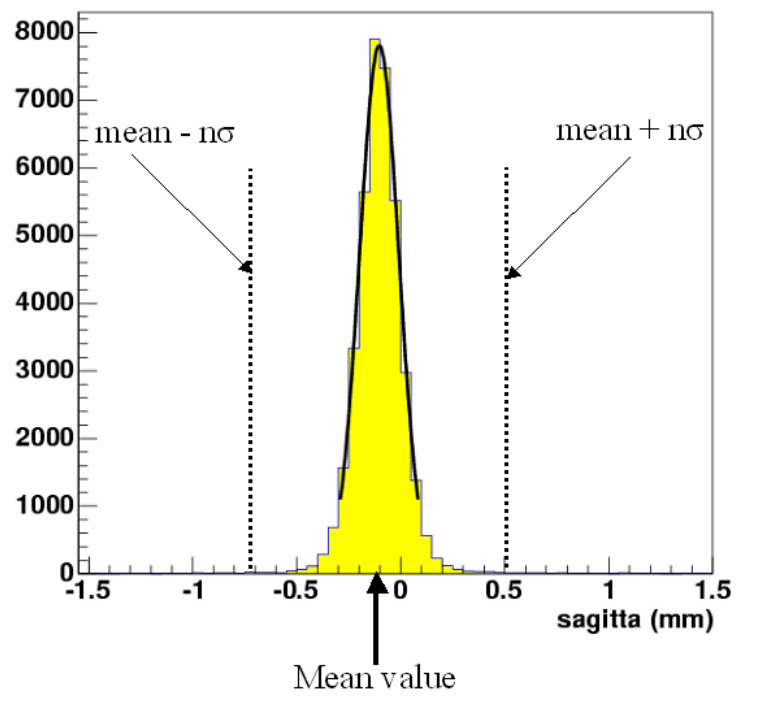

Figure 31: The *sagitta* distribution for a tested chamber. The selected area in which good segments are counted is indicated.

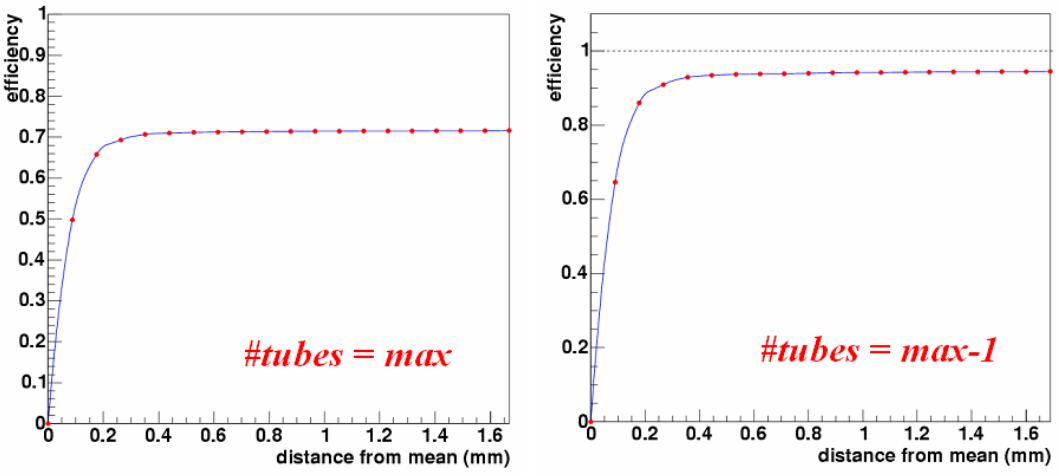

Figure 32: Track segment efficiency, for max and max-1 number of hits, as a function of the distance from the mean value of sagitta distribution.

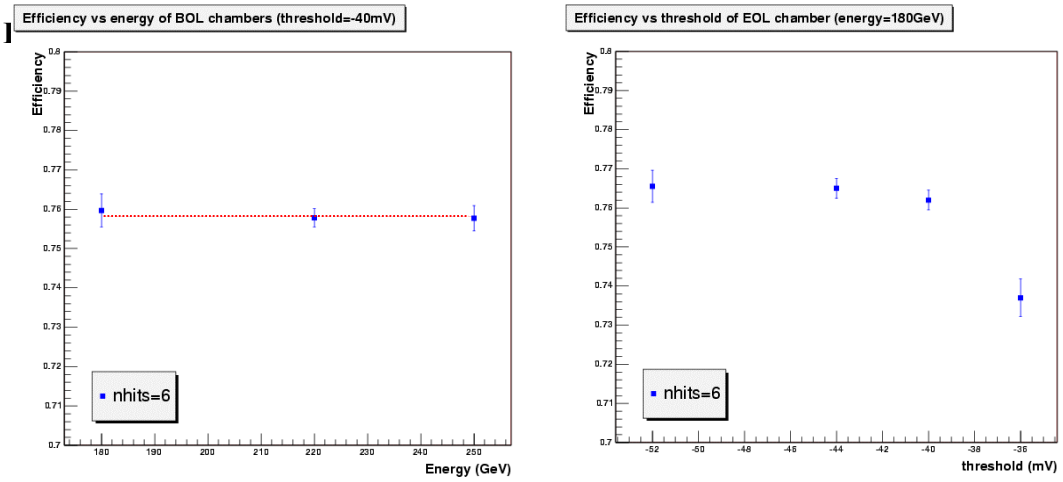

a **b**

Figure 33: a) Track segment efficiency versus energy, for the BOL chamber and for the nominal MDT threshold (- 40mV). b) Track segment efficiency versus MDT threshold of the EOL chamber. The beam energy is 180 GeV.

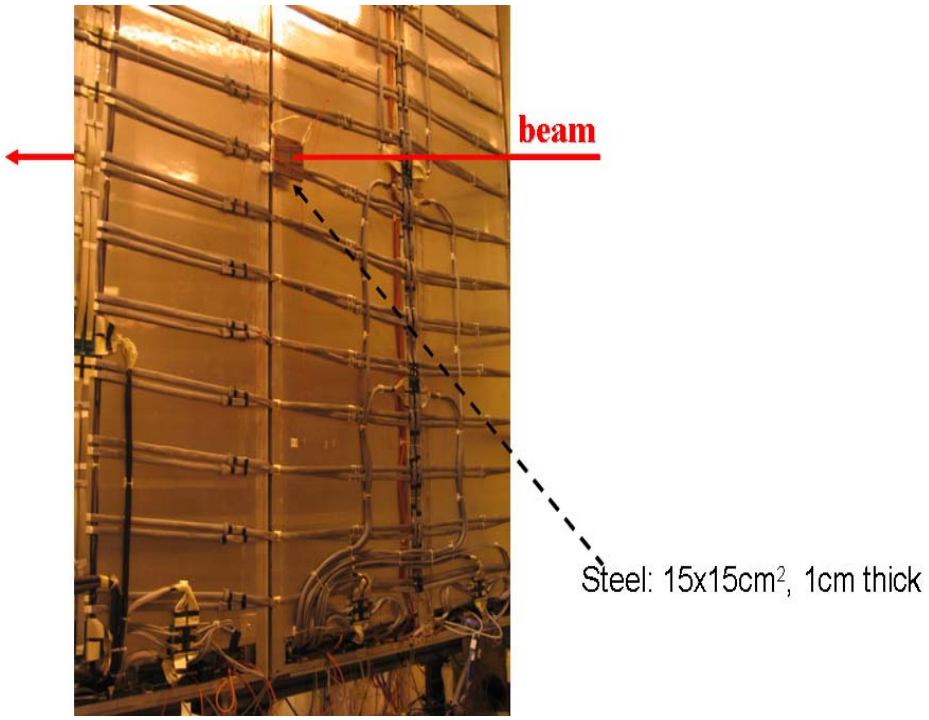

Figure 34: View of BML chambers with a (15 cm x 15 cm x 1 cm) stainless steel block in front.

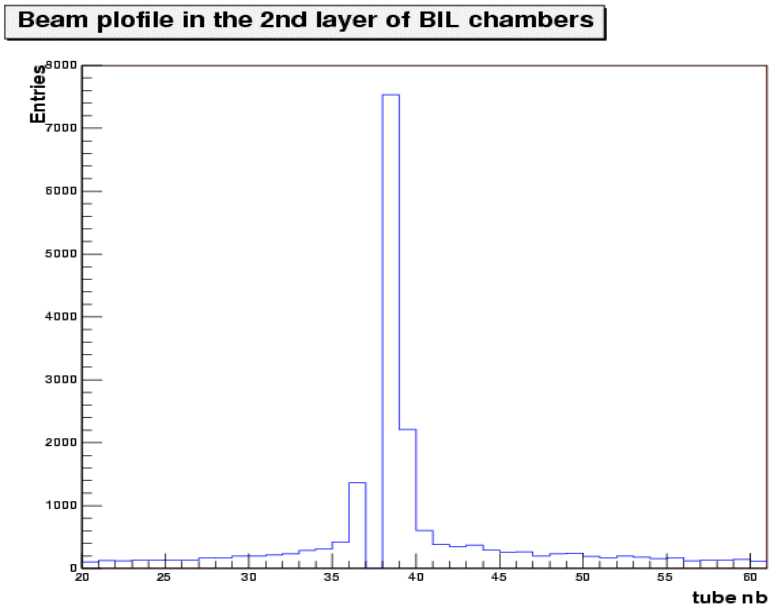

Figure 35: Beam profile in BIL chambers. A dead channel is visible.

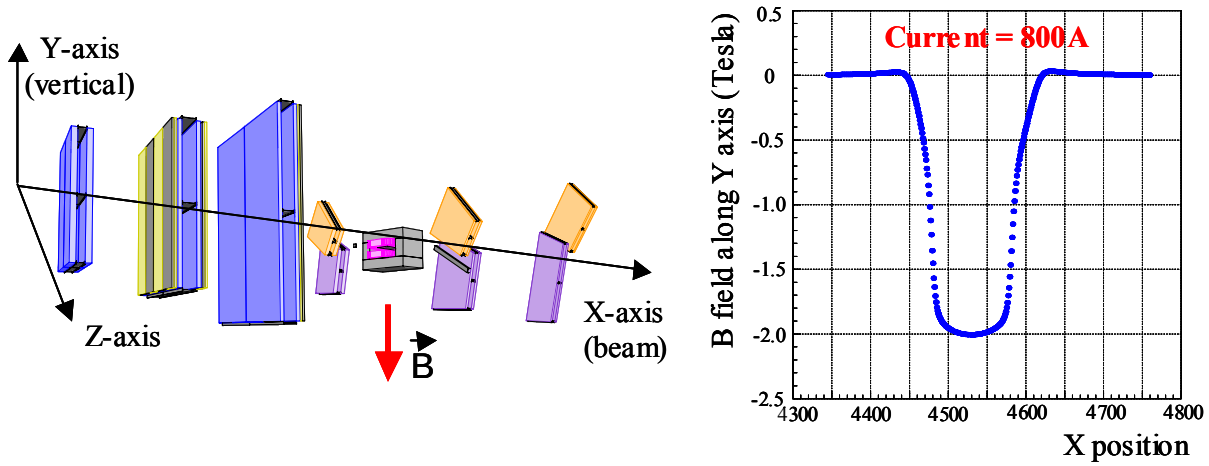

Figure 36: Left plot: *Persint* view of the reference axis and the direction of the B field in the Muon System. Right plot: component of the B-field along the y-axis, as a function of the position along the beam axis (x). The magnet current was set to 800 A.

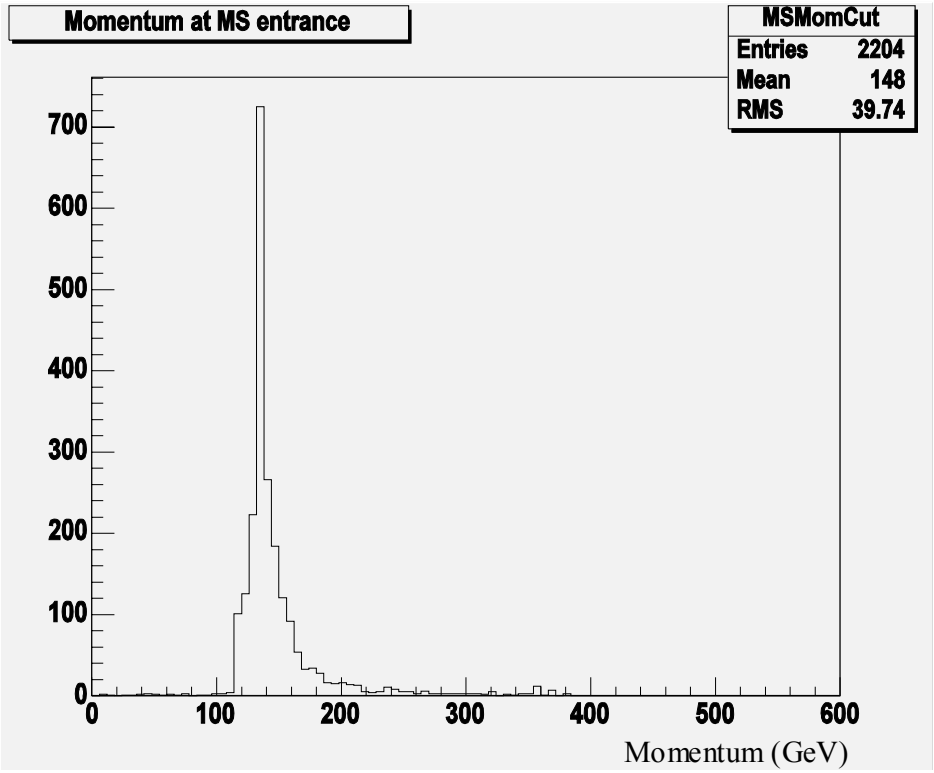

Figure 37: Muon momentum reconstructed using the value of the magnetic field.

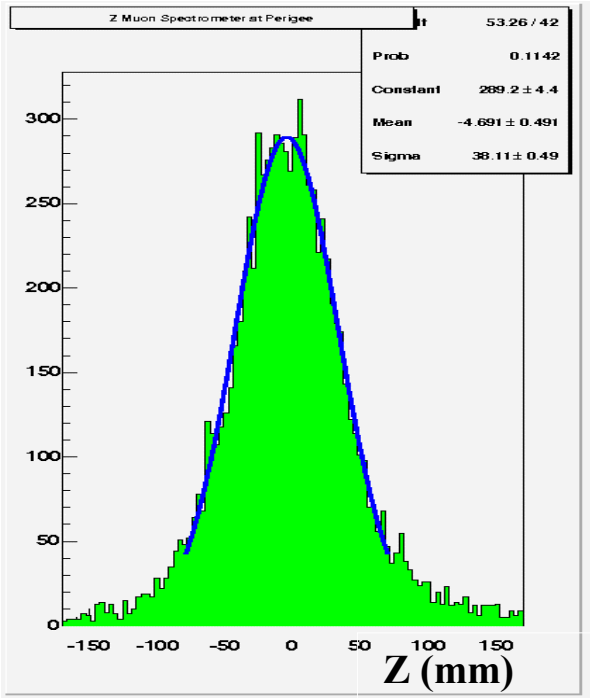

Figure 38: Distribution of the z coordinate of the muon tracks from the muon system extrapolated to perigee.

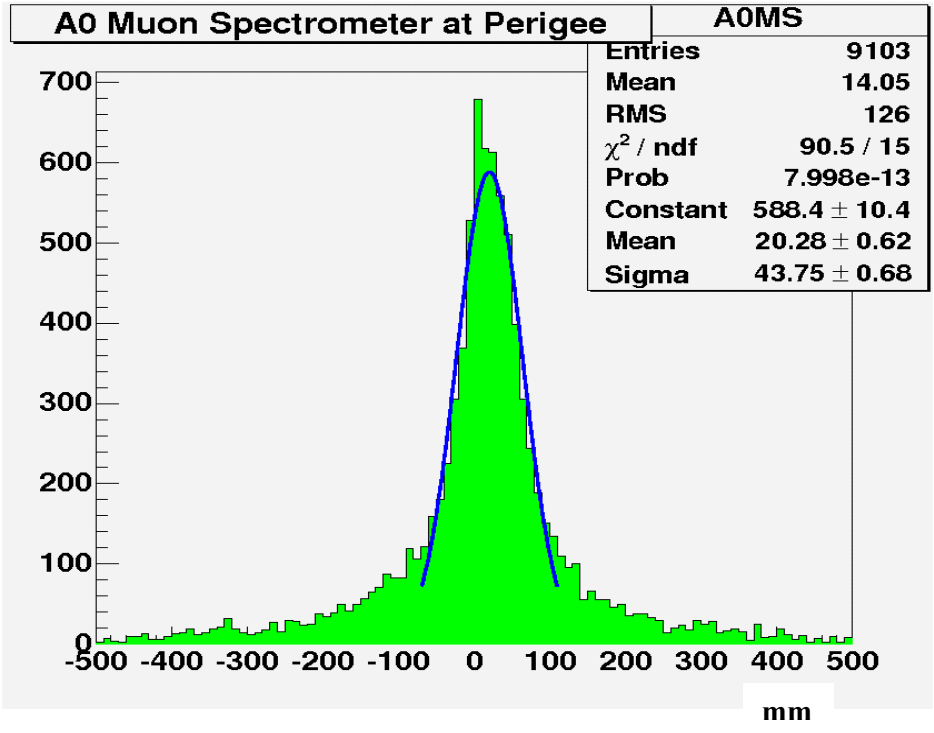

Figure 39: Impact parameter of the muon tracks from the muon system extrapolated to perigee.

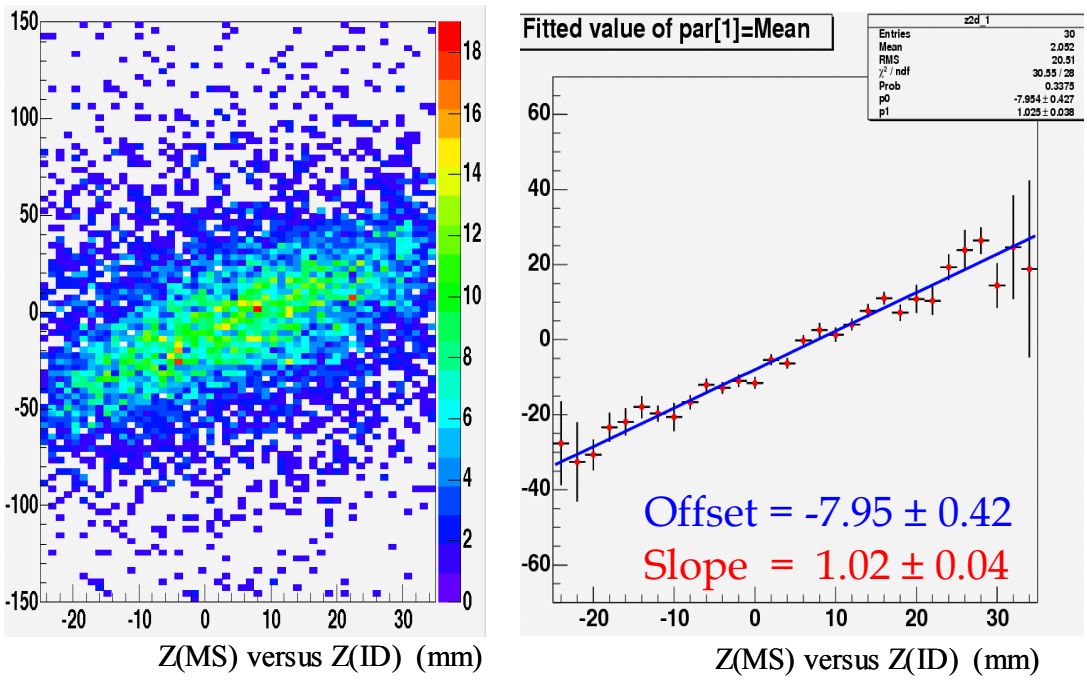

Figure 40: The correlation between the muon system (MS) tracking and the tracking in the inner detector (ID = Pixels and SCT tracking).

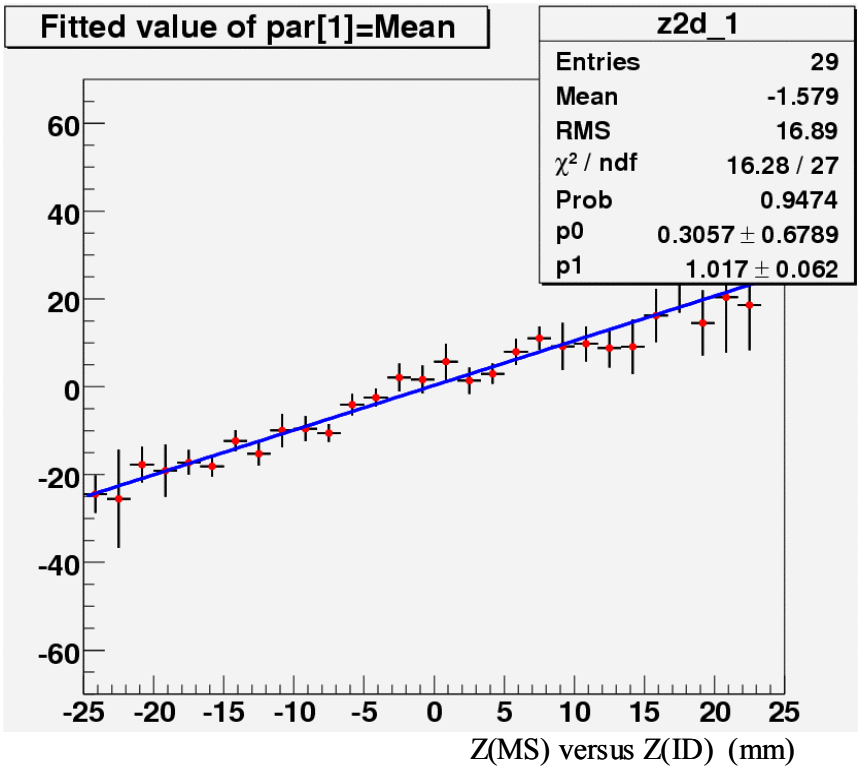

Figure 41: z (MS) versus z (ID), after alignment of the inner detector with respect to the muon system.